

1 **Expansion of oil palm and other cash crops causes an increase of land surface temperature**
2 **of the Jambi province in Indonesia**

3
4 Clifton R. Sabajo^{1,2†}, Gueric le Maire³, Tania June⁴, Ana Meijide¹, Olivier Roupsard^{3,5},
5 Alexander Knohl^{1,6}

6
7 ¹ University of Goettingen, Bioclimatology, 37077 Göttingen, Germany

8 ² AgroParisTech – Centre de Montpellier, Agropolis International, 648 rue Jean-François
9 Breton, 34093 Montpellier, France

10 ³ CIRAD, UMR Eco&Sols, F-34398 Montpellier, France

11 ⁴ Agrometeorology Laboratory Department of Geophysics and Meteorology,

12 Faculty of Mathematics and Natural Sciences, Bogor Agricultural University (IPB), Indonesia

13 ⁵ CATIE (Centro Agronómico Tropical de Investigación y Enseñanza / Tropical Agriculture
14 Centre for Research and Higher Education), 7170 Turrialba, Costa Rica

15 ⁶ University of Goettingen, Centre of Biodiversity and Sustainable Land Use (CBL), 37073
16 Goettingen, Germany

17

18 † Correspondence: Clifton R. Sabajo, University of Goettingen, Bioclimatology, Büsgenweg 2,
19 37077 Göttingen, Germany. E-mail: csabajo@uni-goettingen.de

20 Telephone: +49 (0) 551 39 12114

21

22

23 **Abstract**

24

25 Indonesia is currently one of the regions with the highest transformation rate of the land surface
26 worldwide due to the expansion of oil palm plantations and other cash crops replacing forests
27 on large scales. Land cover changes, which modify land surface properties, have a direct effect

28 on the land surface temperature (LST), a key driver for many ecological functions. Despite the
29 large historic land transformation in Indonesia toward oil palm and other cash crops and
30 governmental plans for future expansion, this is the first study so far to quantify the impact of
31 land transformation in Indonesia on LST. We analyse LST from the thermal band of a Landsat
32 image and produce a high-resolution surface temperature map (30m) for the lowlands of the
33 Jambi province in Sumatra (Indonesia), a region which suffered large land transformation
34 towards oil palm and other cash crops over the past decades. The comparison of LST, albedo,
35 Normalized Differenced Vegetation Index (NDVI), and evapotranspiration (ET) between seven
36 different land cover types (forest, urban areas, clear cut land, young and mature oil palm
37 plantations, acacia and rubber plantations) shows that forests have lower surface temperatures
38 than these land cover types, indicating a local warming effect after forest conversion. LST
39 differences were up to 10.09 ± 2.6 °C (mean \pm SD) between forest and clear-cut land. The
40 differences in surface temperatures are explained by an evaporative cooling effect, which
41 offsets the albedo warming effect. Our analysis of the LST trend of the past 16 years based on
42 MODIS data, shows that the average daytime surface temperature of the Jambi province
43 increased by 1.05 °C, which followed the trend of observed land cover changes and exceed the
44 effects of climate warming. This study provides evidence that the expansion of oil palm
45 plantations and other cash crops leads to changes in biophysical variables, warming the land
46 surface and thus enhancing the increase in air temperature due to climate change.

47

48

49 *Keywords:* Land surface temperature, albedo, NDVI, evapotranspiration, biophysical variables,
50 oil palm, remote sensing, Landsat, MODIS, Indonesia, land-use / land cover change

51

52

53 **1 Introduction**

54

55 Indonesia is one of the regions where the expansion of cash crop monocultures such as acacia
56 (timber plantation), rubber, oil palm plantations and smallholder agriculture has drastically
57 reduced the area of primary forest in the last two and a half decades (Bridhikitti and Overcamp,
58 2012; Drescher et al., 2016; Marlier et al., 2015; Miettinen et al., 2012; Verstraeten et al., 2005).
59 This large scale conversion of rainforest for agricultural use has been observed on the island of
60 Sumatra, which has experienced the highest primary rainforest cover loss in all of Indonesia
61 (Drescher et al., 2016; Margono et al., 2012; Miettinen et al., 2011). Forest cover in the
62 Sumatran provinces of Riau, North Sumatra and Jambi, declined from 93 to 38% of provincial
63 area between 1977 and 2009 (Miettinen et al., 2012). These large scale transformations,
64 observed as land cover change, and land-use intensification have led to substantial losses in
65 animal and plant diversity, and ecosystem functions and changed microclimatic conditions
66 (Clough et al., 2016; Dislich et al., 2016; Drescher et al., 2016). Additionally, these changes
67 directly alter vegetation cover and structure as well as land surface properties such as albedo,
68 emissivity, and surface roughness which affect gas and energy exchange processes between the
69 land surface and the atmosphere (Bright et al., 2015).

70

71 Replacing natural vegetation with another land cover modifies the surface albedo, which affects
72 the amount of solar radiation that is absorbed or reflected and consequently alters net radiation
73 and local surface energy balance. A lower or higher albedo results in a smaller or greater
74 reflection of shortwave radiation. As a result, the higher or lower amounts of net radiation
75 absorption may increase or decrease the surface temperature and change evapotranspiration
76 (Mahmood et al., 2014).

77

78 Changes in land cover also alter surface emissivity, i.e. the ratio of radiation emitted from a
79 surface to the radiation emitted from an ideal black body at the same temperature following the
80 Stefan–Boltzmann law. Emissivity of vegetated surfaces varies with plant species, density,
81 growth stage, water content and surface roughness (Snyder et al., 1998; Weng et al., 2004). A
82 change of emissivity affects the net radiation because it determines the emission of longwave
83 radiation that contributes to radiative cooling (Mahmood et al., 2014).

84

85 Water availability, surface type, soil humidity, local atmospheric and surface conditions affect
86 the energy partitioning into latent (LE), sensible (H) and ground heat (G) fluxes (Mildrexler et
87 al., 2011). Surface roughness affect the transferred sensible and latent heat by regulating vertical
88 mixing of air in the surface layer (van Leeuwen et al., 2011) thereby regulating land surface
89 temperature (LST). Through its association with microclimate, net radiation and energy
90 exchange (Coll et al., 2009; Sobrino et al., 2006; Voogt and Oke, 1998; Weng, 2009; Zhou and
91 Wang, 2011), LST is a major land surface parameter that also influences habitat quality and
92 thus the distribution of plants and animals and biodiversity.

93

94 The replacement of natural vegetation also changes evapotranspiration (ET) (Boisier et al.,
95 2014). When ET decreases, surface temperatures and fluxes of sensible heat (H) increase. On
96 the other hand, when ET increases, the increased LE fluxes lower surface temperatures and
97 decrease H fluxes (Mahmood et al., 2014). Vegetation structure as reflected by parameters such
98 as the Normalized Difference Vegetation Index (NDVI), Leaf Area Index (LAI) and vegetation
99 height is in this respect an important determinant of the resistances or conductivities to heat,
100 moisture, and momentum transfer between the canopy and the atmosphere (Bright et al., 2015)
101 facilitating the amounts/ratios of sensible heat to water vapour dissipation away from the
102 surface (Hoffmann and Jackson, 2000).

103

104 Surface albedo, surface temperature, surface emissivity, and indirectly LAI and NDVI are
105 interconnected through the surface radiation balance. When the land surface is changed,
106 feedback mechanisms involving these biophysical variables control the radiation balance and
107 the surface temperature.

108 To understand the effects of land cover changes on LST, the associated biophysical variables
109 must be evaluated. This can be done through the surface radiation budget and energy
110 partitioning which unites these biophysical variables directly or indirectly: albedo as direct
111 determinant of the net solar radiation, NDVI as a vegetation parameter determining the
112 emissivity, which in turn determines the amount of reflected and emitted longwave radiation,
113 LST directly affecting the amount of emitted longwave radiation from the surface and ET,
114 which affects the amount of energy that is used for surface cooling via evaporating of water.

115

116 The effect of land cover change on LST is dependent on the scale, location, direction and type
117 of the change (Longobardi et al., 2016). Several studies showed an increase of the LST after
118 forest conversion to built-up areas and agricultural land (Zhou and Wang, 2011) and to crop
119 land and pasture lands (Peng et al., 2014) in China. Similar findings were reported for South
120 American ecosystems: low vegetation such as grasslands in Argentina were warmer than tall
121 tree vegetation (Nosetto et al., 2005). In Brazil, the surface temperature increased after the
122 conversion of natural Cerrado vegetation (a savanna ecosystem) into crop/pasture (Loarie et al.,
123 2011a). Similar effects were also shown for other South American biomes (Salazar et al., 2016).
124 In a global analysis, Li et al. (2015) showed that the cooling of forests is moderate at mid
125 latitudes and that Northern boreal forests are even warmer, an indication that the effect of land
126 cover change on LST varies with the location of the land cover change (Longobardi et al.,
127 2016). Similar studies on the Indonesian Islands are lacking but increases in surface temperature
128 are expected as an effect of the expansion of oil palm and cash crop land in the recent decades.

129

130 Measuring changes in LST is critical for understanding the effects of land cover changes, but
131 challenging. LST can be monitored with LST products retrieved from thermal infrared (TIR)
132 remote sensing data e.g. the use of the thermal bands of the Moderate Resolution Imaging
133 Spectrometer (MODIS) onboard the Terra and Aqua satellite (Sobrino et al., 2008), the thermal
134 band of the Thematic Mapper (TM) onboard the LANDSAT-5 platform (Sobrino et al., 2004,
135 2008) or Enhanced Thematic Mapper (ETM+) onboard the LANDSAT-7 platform. The
136 advantage of MODIS data is the availability of readily processed products at high temporal
137 resolution (daily) at medium (250 – 500 m) to coarse spatial resolution (1000 – 5000 m) scale;
138 MODIS LST product (MOD11A1/MYD11A1) for example is provided at a daily temporal
139 resolution with a spatial resolution of 1 km. Landsat data are provided at a higher spatial
140 resolution (30 m), but its temporal resolution is however limited to 16 days and the retrieval of
141 LST requires the correction of the satellite observed radiances for atmospheric absorption and
142 emission (Coll et al., 2009). Besides LST, the connected biophysical variables of the energy
143 and radiation budget can be derived from the visible and near-infrared (VIS-NIR) bands of
144 either MODIS or Landsat, making integrated monitoring of the biophysical variables related to
145 changing land surface possible. In Indonesia, a large proportion of the land use changes is
146 driven by smallholders (Dislich et al. 2016), thus a combination of Landsat (for a fine spatial
147 resolution) and MODIS (for temporal developments) seems desirable.

148

149 The modification of the physical properties of the land surface influences climate/local
150 microclimatic conditions via biogeochemical and biophysical processes. Therefore, given
151 Indonesia's history of large scale agricultural land conversion and governmental plans to
152 substantially expand the oil palm production, it is important to study the effect of the expansion
153 of cash crop areas on the biophysical environment, especially on LST as a key land surface
154 parameter. These effects have been poorly studied in this region and according to our
155 knowledge this is the first study to quantify the effects of land use change on LST in Indonesia

156 We focus on the province of Jambi / Sumatra as it experienced large land transformation
157 towards oil palm and other cash crops such as rubber plantations in the past and it may serve as
158 an example of future changes in other regions.

159

160 Our main objective is to quantify the differences in LST across different land cover types and
161 to assess the impact of cash crop expansion on the surface temperature of Jambi province (on
162 Sumatra / Indonesia) in the past decades. With this study we aim to (1) evaluate the use of
163 Landsat and MODIS satellite data as sources for a reliable estimation of the surface temperature
164 in a tropical region with limited satellite data coverage by comparing the surface temperatures
165 retrieved from both satellite sources to each other and against ground observations, (2) to
166 quantify the LST variability across different land cover types and (3) to assess the long term
167 effects of land transformation on the surface temperature against the background of climatic
168 changes and (4) to identify the mechanisms that explain changes of the surface temperature
169 through changes in other biophysical variables. In this study we compare the surface
170 temperatures of different land cover types that replace forests (i.e. oil palm, rubber and acacia
171 plantations, clear cut land and urban areas) using high resolution Landsat and medium
172 resolution MODIS satellite data and discuss the differences by taking into account other
173 biophysical variables such as the albedo, NDVI and evapotranspiration (ET).

174

175 **2 Materials and methods**

176

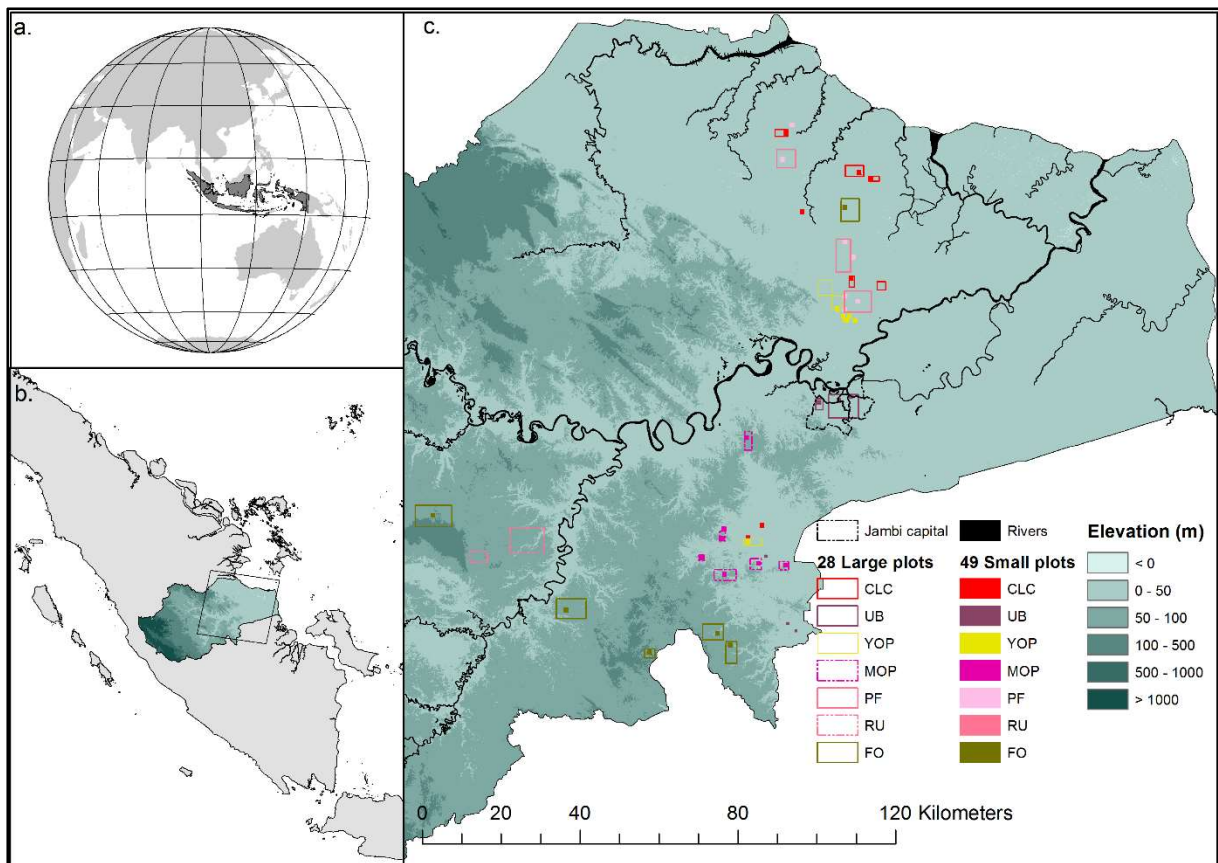
177 **2.1 Study area**

178

179 The study was carried out in the lowlands (approx. 25 000 km²) of the Jambi province (total
180 area 50 160 km²) on Sumatra, Indonesia, between latitudes 0°30'S and 2°30'S and longitudes
181 101°E and 104°30'E (Fig. 1). This region has undergone large land transformation towards oil

182 palm and rubber plantation over the past decades and thus may serve as an example of expected
183 changes in other regions of Indonesia (Drescher et al. 2016). The area has a humid tropical
184 climate with a mean annual temperature of 26.7 ± 0.2 °C (1991 – 2011, annual mean \pm SD of
185 the annual mean), with little intra-annual variation. Mean annual precipitation was 2235 ± 381
186 mm and a dry season with less than 120 mm monthly precipitation usually occurred between
187 June and September (Drescher et al., 2016). Previously logged rainforests in the Jambi province
188 have been converted to intensively managed agro-industrial production zones as well as into
189 smallholder farms to grow cash crops tree of rubber (*Hevea brasiliensis*) and oil palm (*Elaeis*
190 *guineensis*) or fast-growing tree species such as *Acacia mangium* for pulp production (Drescher
191 et al., 2016). The area cultivated with oil palm grew faster than the area cultivated with rubber
192 plantations between 1990 and 2011 (Clough et al. 2016).

193
194 For this study, we used two data sets of different plot sizes. For the first data set, we delineated
195 28 large plots (ranging from 4 to 84 km²) of 7 different land cover types (Forest (FO), Rubber
196 (RU), Acacia Plantation Forest (PF), Young oil palm plantation (YOP), Mature Oil Palm
197 Plantation (MOP), Urban area (UB) and Clear-Cut areas (CLC)) (Fig. 1). The delineation was
198 based on visual interpretation in combination with information from field work, which was
199 carried out between October – December 2013. The large size of the plots was necessary to
200 make a comparison between MODIS and Landsat images (see section satellite data). For the
201 second data set, we selected 49 smaller plots within and outside these 28 large plots (between
202 50 × 50 m and 1000 × 1000 m) (Fig. 1) which allowed us to increase the number of plots to use
203 when analysing Landsat images. These small plots were used to extract surface temperature
204 (LST), Normalized Difference Vegetation Index (NDVI), albedo (α) and evapotranspiration
205 (ET) from a high resolution Landsat satellite image (see section satellite data) for the 7 different
206 land cover types of interest.



207
 208 **Fig. 1** Geographic location of the study area. Jambi province on the Sumatran Island of
 209 Indonesia (Figs. 1a and 1b). The background of the map (Fig. 1c) is a digital elevation model,
 210 showing that the plots are located in the lowlands of the Jambi province. The large rectangles
 211 are the 28 different land cover types (Forest, Young and Mature Oil palm, Rubber, Urban area,
 212 Acacia Plantation Forest and Clear-Cut land), the small squares are the locations of the 49 small
 213 plots of the 7 different land cover types. Abbreviations: CLC = Clear-cut land, UB = Urban
 214 area, YOP = Young oil palm plantation, MOP = Mature Oil Palm plantation, PF = Acacia
 215 plantation forest, RU = Rubber plantation, FO = Forest.

216
 217 **2.2 Meteorological data**
 218

219 Air temperature and relative air humidity were measured at four reference meteorological
 220 stations located in open areas within the area of study (Drescher et al., 2016), with
 221 thermohygrometers (type 1.1025.55.000, Thies Clima, Göttingen, Germany) placed at 2m
 222 height. Measurements were taken every 15 s and then averaged and stored in a DL16 Pro data

223 logger (Thies Clima, Göttingen, Germany) as 10 min mean, from February 2013 to December
224 2015. We used the air temperature from the meteorological stations to compare to MODIS air
225 temperatures (MOD07_L2). The relative air humidity was used as an input parameter for
226 NASA's online atmospheric correction (ATCOR) parameter tool to derive parameters to correct
227 Landsat thermal band for atmospheric effects (see Satellite data). We also used air temperature
228 and relative humidity from two eddy covariance flux towers located in the study area (Meijide
229 et al., 2017) one in a young oil palm plantation (two years old, S 01°50.127', E 103°17.737'),
230 and the other one in a mature oil palm plantation (twelve years old, S 01°41.584', E
231 103°23.484'). At these flux towers, air temperature and relative humidity were measured above
232 the canopy respectively with the same instruments as in the reference meteorological stations
233 (see (Meijide et al., 2017), for description of methodology). In the flux tower located in the
234 mature oil palm plantation, we also measured surface canopy temperature between August 2014
235 and December 2015, which was compared to MODIS LST estimates from the same period.
236 Measurements of canopy temperature were performed with two infrared sensors (IR100)
237 connected to a data logger, (CR3000) both from Campbell Scientific Inc. (Logan, USA). For a
238 regional coverage we used ERA Interim daily air temperature grids
239 (<http://apps.ecmwf.int/datasets/data/interim-full-daily/levtype=sfc/>; (Dee et al., 2011) from
240 2000 – 2015 at 0.125 degrees resolution to study the annual air temperature trend in this period.

241

242 **2.3 Satellite data**

243

244 A Landsat 7 ETM+ VIS/TIR 30 m resolution surface reflectance image with low cloud cover,
245 acquired at 10:13 hours (local time) on 19 June 2013 covering the lowland area of the Jambi
246 province (path 125, row 61) was used in this study. Like all Landsat 7 ETM+ images acquired
247 after 31 May 2003, the image we used was affected by a scan line error causing a data loss of
248 about 22% (http://landsat.usgs.gov/products_slcoffbackground.php). Most selected plots were

249 located in the center of the image and thus not affected by the data loss, e.g. the forest plots
250 located at the edges of the scan line error zone faced minimal data loss because they were large
251 enough.

252 We also downloaded the tile h28v09 of the MODIS Terra (MOD) and Aqua (MYD) daily 1km
253 Land Surface Temperature and Emissivity products (MOD11A1 and MYD11A1 Collection-5)
254 and MODIS 16-days 500 m Vegetation Indices NDVI/EVI product (MOD13A1 Collection-5)
255 from 05 March 2000 till 31 December 2015 for Terra data and from 8 July 2002 till 31
256 December 2015 for Aqua data. We downloaded other supporting satellite data such as the
257 MODIS Atmospheric Profile product (MOD07_L2) and the MODIS Geolocation product
258 (MOD03). All MODIS data were reprojected to WGS84, UTM zone 48 South using the MODIS
259 Reprojection Tool (MRT). The quality of the MODIS data was checked using the provided
260 quality flags and only pixels with the highest quality flag were used in the analysis.

261

262 **2.4 Retrieval of biophysical variables from Landsat 7 ETM+ VIS/TIR images**

263

264

- 265 • *NDVI*

266

267 NDVI was derived using the reflectances corrected for atmospheric effects in the red (ρ_{RED} ,
268 band 3 Landsat 7 ETM+) and near infrared (ρ_{NIR} , band 4 Landsat 7 ETM+) bands, with:

269

270

$$271 \quad NDVI = \frac{\rho_{NIR} - \rho_{RED}}{\rho_{NIR} + \rho_{RED}} \quad (1)$$

272

273 • *Surface albedo*

274

275 The surface albedo (α) was computed using the equation of Liang (2000) for estimating
276 broadband albedo from Landsat surface reflectance bands, with:

277

$$278 \alpha = 0.3141 \rho_1 + 0.1607 \rho_3 + 0.369 \rho_4 + 0.1160 \rho_5 + 0.0456 \rho_7 - 0.0057 \quad (2)$$

279

280 where ρ_1 , ρ_3 , ρ_4 , ρ_5 and ρ_7 are the Landsat 7 ETM+ surface reflectance bands (corrected for
281 atmospheric effects).

282

283 • *Surface temperature (LST)*

284

285 LST was derived following the method proposed by Bastiaanssen (2000), Bastiaanssen et al.
286 (1998a), Coll et al. (2010) and Wukelic et al. (1989) for computing the surface temperature
287 from the thermal infrared band (TIR, band 6) of Landsat (Supporting information, S1). The
288 thermal infrared band (TIR, band 6) was first converted to thermal radiance (L6, $W/m^2/sr/\mu m$)
289 and then to atmospherically corrected thermal radiance (R_c , $W/m^2/sr/\mu m$) following the method
290 described by Wukelic et al. (1989) and Coll et al. (2010), and using the atmospheric parameters
291 obtained on NASA's online Atmospheric Correction Calculator (Barsi et al., 2003, 2005)
292 (supporting information, S2). The surface temperature (LST, K) was computed through the
293 following equation similar to the Planck equation, as in Coll et al. (2010) and Wukelic et al.
294 (1989):

295

296
$$LST = \frac{k_2}{\ln\left(\frac{\epsilon_{NB} \cdot k_1}{R_c} + 1\right)}$$
 (3)

297

298 where ϵ_{NB} is the emissivity of the surface obtained from the NDVI (Supporting information,
299 Table S1), k_1 (= 666.09 mW/cm²/sr/μm) and k_2 (= 1282.71 K) are sensor constants for
300 converting the thermal radiance obtained from band 6 of Landsat 7 to surface temperature.

301 The surface temperature derived from Landsat thermal band was compared with a MODIS LST
302 product that was acquired on the same day at 10:30 am local time. For this, the Landsat LST
303 image was resampled to MODIS resolution to enable a pixel to pixel comparison, followed by
304 extracting the average LST of 7 land cover types using the data set containing the large
305 delineated plots (Fig. 1).

306

307 • *Evapotranspiration (ET)*

308

309 Based on the Surface Energy Balance Algorithm for Land (SEBAL) (Bastiaanssen, 2000;
310 Bastiaanssen et al., 1998a, 1998b) we estimated ET (mm/hr) from latent heat fluxes (LE, W/m²)
311 which were computed as the residual from sensible (H, W/m²) and ground (G, W/m²) heat
312 fluxes subtracted from net radiation (Rn, W/m²) as:

313

314
$$LE = R_n - G - H$$
 (4)

315

316 We calculated Rn as the sum of incoming shortwave and longwave radiation, minus the
317 reflected shortwave and longwave radiation and the emitted longwave radiation (equation 5).

318 The surface albedo, surface emissivity and surface temperature determine the amounts of
319 incoming and reflected radiation:

320

321 $R_n = (1 - \alpha) S_{d\downarrow} + \epsilon_a \sigma T_a^4 - (1 - \epsilon_0) \epsilon_a \sigma T_a^4 - \epsilon_0 \sigma LST^4$ (5)

322

323 Where $S_{d\downarrow}$ is the incoming shortwave solar radiation (W/m^2) at the surface; α is the surface
 324 albedo (equation 2); ϵ_0 is the surface emissivity (-); ϵ_a is the atmospheric emissivity (-); σ is the
 325 Stephan-Boltzmann constant ($5.67 \times 10^{-8} W/m^2/K^4$); LST is the surface temperature (K,
 326 equation 3); T_a is the near surface air temperature (K). The surface emissivity (ϵ_0) is derived
 327 from the NDVI and is described in the supporting information (Table S1). The average
 328 atmospheric emissivity (ϵ_a) is estimated with the model of Idso and Jackson (1969):

329

330 $\epsilon_a = 1 - 0.26 \cdot \exp \{(-7.77 \times 10^{-4}) \cdot (273.15 - T_a)^2\}$ (6)

331

332 Ground heat fluxes (G , W/m^2) were derived as a fraction of R_n from an empirical relationship
 333 between LST, α , and NDVI (Bastiaanssen, 2000) as:

334

335 $G = R_n \cdot \frac{LST - 273.15}{\alpha} \cdot (0.0038\alpha + 0.0074\alpha^2) \cdot (1 - 0.98NDVI^4)$ (7)

336

337 In SEBAL Sensible heat flux (H , W/m^2) was calculated as:

338

339 $H = \rho C_p \frac{\Delta T}{r_{ah}} = \rho C_p \frac{a LST + b}{r_{ah}}$ (8)

340

341 Where ρ is the air density ($1.16 kg/m^3$); C_p is the specific heat of air at constant pressure (1004
 342 $J/kg/K$); r_{ah} is the aerodynamic resistance to heat transport ($s m^{-1}$); a and b are regression
 343 coefficients which are determined by a hot extreme pixel (where $LE = 0$ and H is maximum)
 344 and a cold extreme pixel (where $H = 0$ and LE is maximum). The aerodynamic resistance to
 345 heat transport, r_{ah} , is calculated through an iterative process with air temperature measured at 2

346 m as input. SEBAL is described in Bastiaanssen (2000) and Bastiaanssen et al. (1998a, 1998b).
347 The application of SEBAL in this research is briefly described in the supporting information
348 (S3: ET from satellite images).

349

350 **2.5 Local short term differences between different land cover types**

351

352 From the created LST, NDVI, Albedo and ET images we extracted the average values of the
353 different land cover classes. For this we used the dataset containing the small 49 delineated
354 plots covering 7 different land cover types (Fig. 1). The average effect of land transformation,
355 i.e. the change from forest to another non-forest land cover type, on the surface temperature
356 was evaluated as (cf. Li et al. (2015)) :

357

$$358 \Delta LST = LST_{\text{non-forest}} - LST_{\text{forest}} \quad (9)$$

359

360 A negative ΔLST indicates a cooling effect and positive ΔLST indicates a warming effect of
361 the non-forest vegetation compared to forest. The same procedure was applied in evaluating the
362 effect of land transformation on the NDVI, albedo and ET.

363

364 **2.6 Effects of land cover change on the provincial surface temperature in the past decades**

365

366 To analyse the long-term effects on the provincial scale we used the MODIS daily LST time
367 series (MOD11A1 and MYD11A1) from 2000 – 2015. MOD11A1 provides LST for two times
368 of the day: 10:30 am and 10:30 pm and we used the times series between 2000 and 2015.
369 MYD11A1 provides LST for 1:30 am and 1:30 pm and is available from 8 July 2002; we used
370 complete years in our analysis and therefore used the MYD11A1 time series from 2003 – 2015.
371 We calculated the mean annual LST at four different times of the day (10:30 am, 1:30 pm,

372 10:30 pm and 1:30 am) between 2000 and 2015 for the lowland of the Jambi from the MODIS
373 daily LST time series (MOD11A1 and MYD11A1). To do so (1) we calculated for each pixel
374 the average LST pixel value using only the best quality pixels for every year; (2) from these
375 pixels we made a composite image (n = 16, one for each year) for the province and (3) from
376 each composite image we calculated the mean annual lowland provincial temperature as the
377 average of all the pixels that are enclosed by a zone delineating the lowland of the Jambi
378 province. We performed the same analysis with the MODIS 16-day NDVI product (2000 –
379 2015) and the ERA daily temperature grid (2000 – 2015) to compare the annual trends of LST,
380 NDVI and air temperature of the province. The average provincial LST and NDVI were
381 compared to the mean LST and NDVI of a selected forest that remained undisturbed forest
382 during the 2000 – 2015 period.

383

384 **2.7 Statistical analysis**

385

386 For comparison of the Landsat derived LST and the MODIS LST we analyzed the statistical
387 relationships with the coefficient of determination (R^2), the root mean square error (RMSE),
388 the mean absolute error (MAE) and the bias (Bias):

$$389 \text{ RMSE} = \sqrt{\frac{\sum_{i=1}^N (E_i - O_i)^2}{N}} \quad (10)$$

390

$$391 \text{ Bias} = \frac{\sum_{i=1}^N (E_i - O_i)}{N} \quad (11)$$

392

$$393 \text{ MAE} = \frac{\sum_{i=1}^N |E_i - O_i|}{N} \quad (12)$$

394

395 Where O_i is MODIS LST, E_i is the Landsat surface temperature, and N is the number of pixels
396 compared. Model type 2 linear regression was applied for fitting the relation between MODIS
397 LST and Landsat LST.

398 We tested the relation between the biophysical variables LST (or L6 and R_c , both as pre- or
399 intermediate products before obtaining LST), albedo (α), NDVI and ET with correlation
400 analysis and a multiple linear regression was applied to analyse the effects of the biophysical
401 variables on the LST. We used the model: LST (or R_c or L6) $\sim \alpha + NDVI + ET$, and used R^2
402 and standardized β -coefficients to evaluate the strength of the biophysical variables in
403 predicting the LST.

404

405 **3 Results**

406

407 **3.1 Landsat LST compared to MODIS LST**

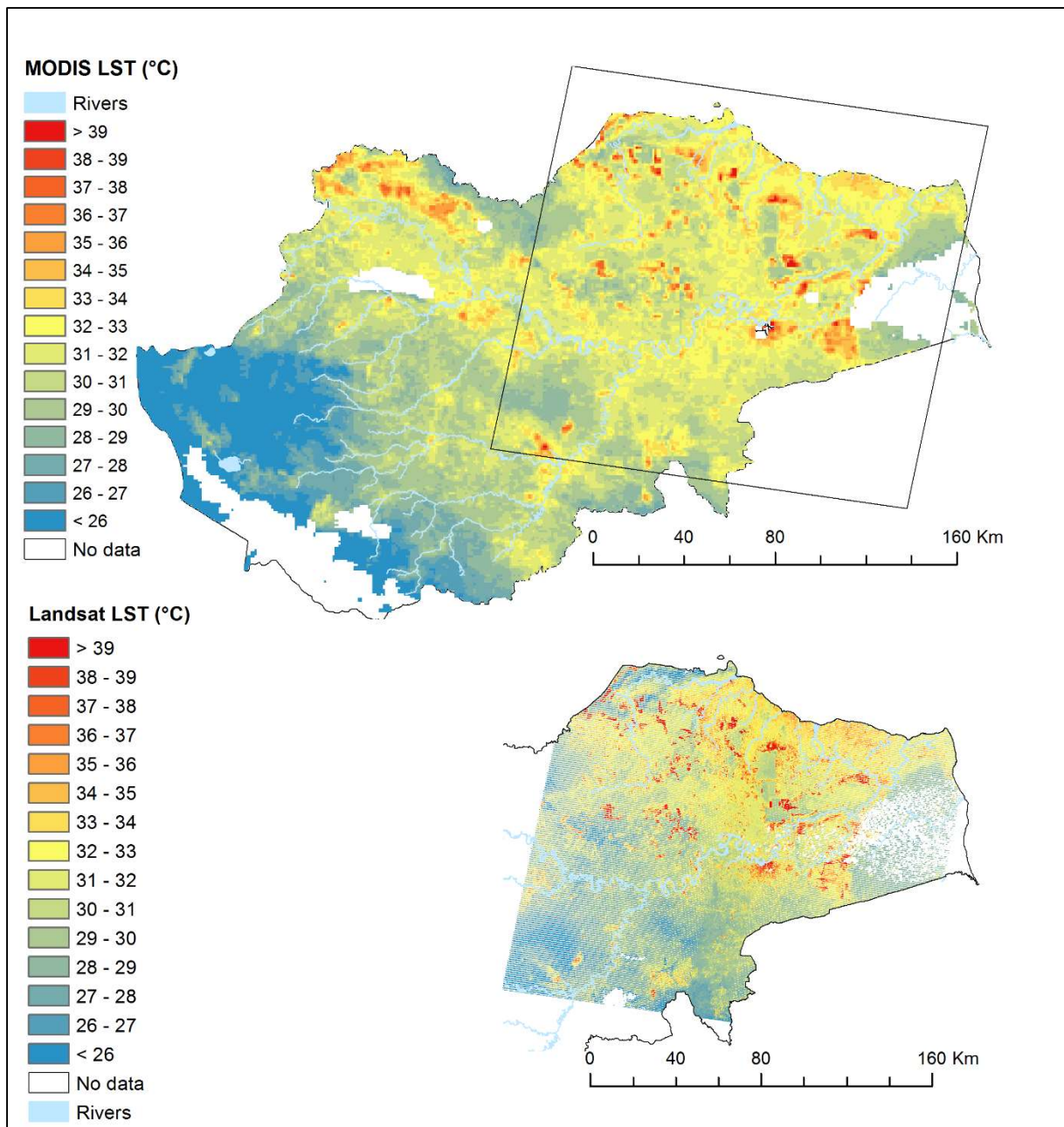
408

409 Landsat and MODIS images showed similar spatial patterns of LST (Fig. 2). In both images the
410 hot areas (red) correspond to the known clear cut areas, urban areas or other sparsely vegetated
411 areas, the cooler areas (blue) correspond to vegetated areas such as forest, plantation forests and
412 mature oil palm plantations. The coarse resolution scale of MODIS (1000 m for LST) allows a
413 large regional coverage of the study area but does not allow to retrieve detailed information on
414 small patches (smaller than 1 km²). On the other hand, Landsat 7 image allows a detailed study
415 of patches that are small enough (as small as 30 x 30 m²), but is affected by the scan line error
416 causing data loss at the edges of the image. In both MODIS and Landsat images clouds and
417 cloud shadows were removed and therefore lead to data gaps in the images.

418

419

420



421
422

423

424 **Fig. 2** MODIS LST image (top) compared with Landsat LST image (bottom). Cloud cover and

425 cloud shadow cover resulted in data gaps (No data). The difference in acquisition time between

426 the images is 15 minutes. The square in the MODIS image is the area that is covered by the

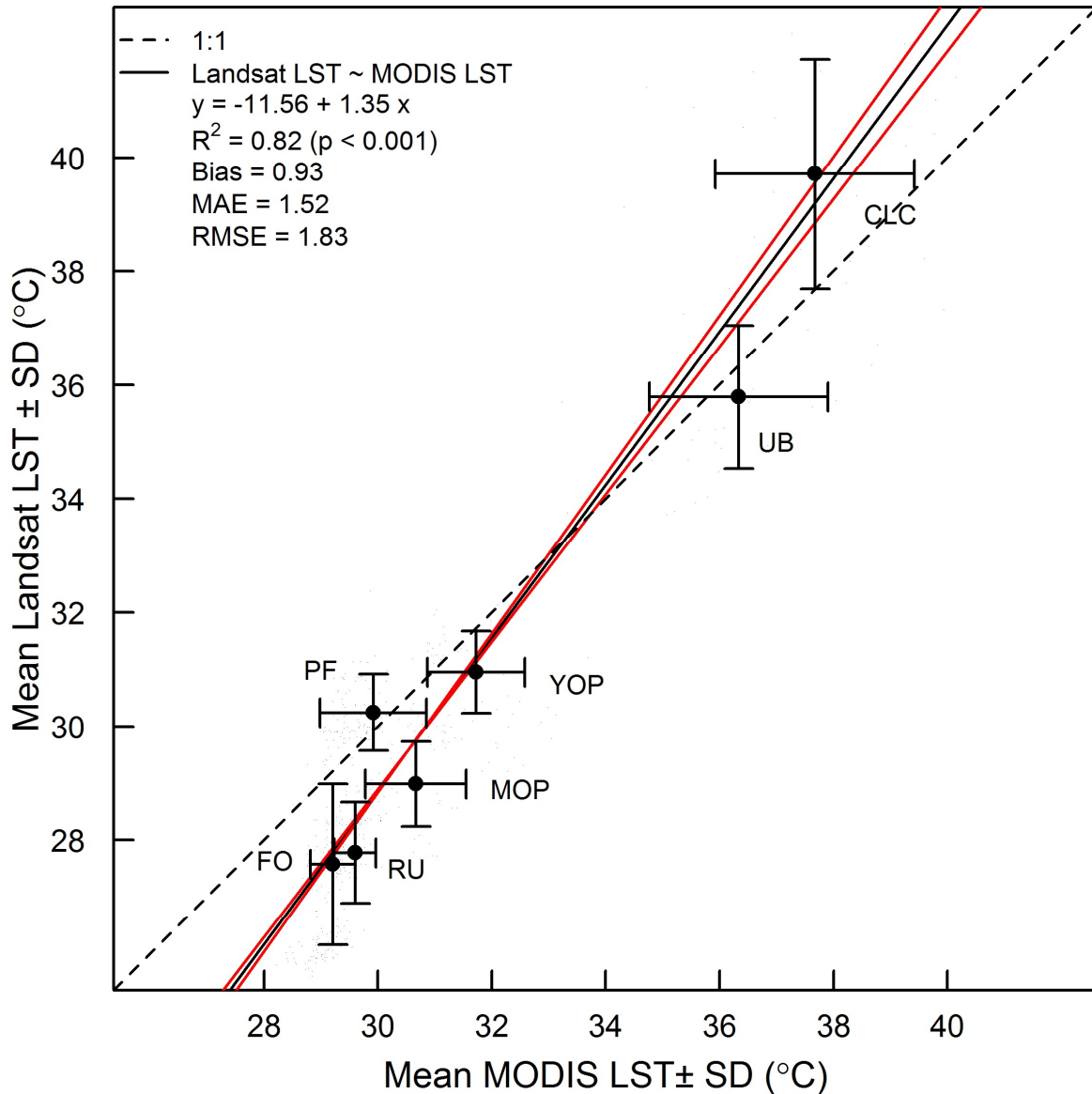
427 Landsat tile (path 125, row 61). Both satellite images were acquired on 19 June 2013.

428

429 Landsat derived LST correlated well with MODIS LST ($R^2 = 0.82$; $p < 0.001$; Fig. 3) with a

430 RMSE of 1.83 °C. The 7 land cover types had distinctive LSTs and the observed differences

431 between these land cover types were consistent in both images. The non-vegetated surfaces
432 (Clear cut land (CLC) and Urban areas (UB)) had higher surface temperatures than the
433 vegetated surface types (FO, YOP, MOP, PF and RU). Clear cut land had the highest surface
434 temperature of all compared land cover types, followed by urban areas whereas the vegetated
435 land cover types had lower surface temperatures: $LST_{CLC} (39.71 \pm 2.01 \text{ }^\circ\text{C}) > LST_{UB} (35.79 \pm$
436 $1.26 \text{ }^\circ\text{C}) > LST_{YOP} (30.95 \pm 0.72 \text{ }^\circ\text{C}) > LST_{PF} (30.25 \pm 0.67 \text{ }^\circ\text{C}) > LST_{MOP} (28.98 \pm 0.75 \text{ }^\circ\text{C})$
437 $> LST_{RU} (27.78 \pm 0.89 \text{ }^\circ\text{C}) > LST_{FO} (27.57 \pm 1.41 \text{ }^\circ\text{C})$ (Landsat LST, Fig. 3). The same trend
438 was derived from the MODIS image but with higher surface temperatures, except for CLC:
439 $LST_{CLC} (37.67 \pm 1.75 \text{ }^\circ\text{C}) > LST_{UB} (36.33 \pm 1.57 \text{ }^\circ\text{C}) > LST_{YOP} (31.73 \pm 0.85 \text{ }^\circ\text{C}) > LST_{MOP}$
440 $(30.67 \pm 0.88 \text{ }^\circ\text{C}) > LST_{PF} (29.92 \pm 0.93 \text{ }^\circ\text{C}) > LST_{RU} (29.60 \pm 0.36 \text{ }^\circ\text{C}) > LST_{FO} (29.21 \pm 0.40$
441 $^\circ\text{C})$ (MODIS LST, Fig. 3).



442
 443 **Fig. 3** Average surface temperature (LST) and standard deviation (SD) of 7 land cover types
 444 derived from Landsat thermal image compared with the mean and SD of MODIS LST.
 445 CLC = Clear cut land, UB = Urban areas, YOP = young oil palm plantation, PF = Acacia
 446 Plantation Forest, MOP = Mature Oil palm plantation, FO = Forest, RU = Rubber plantation.
 447 The dashed line is the theoretical 1:1 line, the solid lines are the Linear Model type 2 regression
 448 line (black) and the confidence limits of the regression line (red). Landsat and MODIS images
 449 were acquired on 19 June 2013, Landsat at 10:13 am local time, MODIS at 10:30 am local time.
 450 Landsat pixels (30 m) were resampled to MODIS pixel resolution (926 m) to make a pixel to

451 pixel comparison between the two sources possible. RMSE is the root mean squared error, MAE
452 is the mean absolute error.

453

454 **3.2 Local short term differences between different land cover types**

455

456 The Δ LST between RU, MOP, PF, YOP, UB and CLC land cover types and FO were all
457 positive, meaning that all other land cover types were warmer than forests (Fig. 4a & Supporting
458 Information S4 and S5). RU and MOP were 0.4 ± 1.5 °C and 0.8 ± 1.2 °C warmer than forest,
459 respectively. PF and YOP were much warmer than forests (Δ LST_{PF-FO} = 2.3 ± 1.1 °C, Δ LST_{YOP}
460 _{-FO} = 6.0 ± 1.9 °C). The largest Δ LSTs were between forest and the non-vegetated land cover
461 types, i.e. UB (Δ LST = 8.5 ± 2.1 °C) and CLC (Δ LST = 10.9 ± 2.6 °C). The LST differences
462 were significant ($p < 0.05$, post-hoc Tukey's HSD test), except between RU and FO ($p = 0.78$,
463 post-hoc Tukey's HSD test (Supporting Information S6, Table S6.1 & table S6.2).

464

465 Similar differences were found for the Δ NDVI between forest and other land covers (Fig. 4b).
466 The negative Δ NDVI indicates that the non-forest land cover types had lower NDVI than forest.
467 Δ NDVI between FO and RU, MOP, PF and YOP were small (between -0.01 ± 0.02
468 (Δ NDVI_{MOP-FO}) and -0.12 ± 0.06 (Δ NDVI_{YOP-FO}). The largest Δ NDVIs were between forest
469 and the non-vegetated land cover types, i.e. UB and CLC (Δ NDVI = -0.42 ± 0.11 and -0.41
470 ± 0.08 , respectively). All Δ NDVIs were significant ($p < 0.05$, post-hoc Tukey's HSD test).

471

472 The difference in albedo (Δ Albedo) between forest and the other land covers was very small
473 (Fig. 4c), with Δ Albedo values between -0.03 ± 0.01 (Δ Albedo_{PF-FO}) and 0.03 ± 0.02
474 (Δ Albedo_{YOP-FO}). These differences were significant ($p < 0.05$, post-hoc Tukey's HSD test).
475 PF had a lower albedo than forest (Δ Albedo_{PF-FO} = -0.03 ± 0.01), while the other land cover
476 types had a higher albedo than forest.

477

478 All land covers had lower ET than forest. RU, MOP and PF had slightly lower ET than FO

479 ($\Delta ET_{RU-FO} = -0.03 \pm 0.04$, $\Delta ET_{MOP-FO} = -0.03 \pm 0.03$ mm/hr, $\Delta ET_{PF-FO} = -0.04 \pm 0.03$ mm/hr)

480 (Fig. 4d). YOP, UB and CLC had much lower ET values than forests: $\Delta ET_{YOP-FO} = -0.18 \pm$

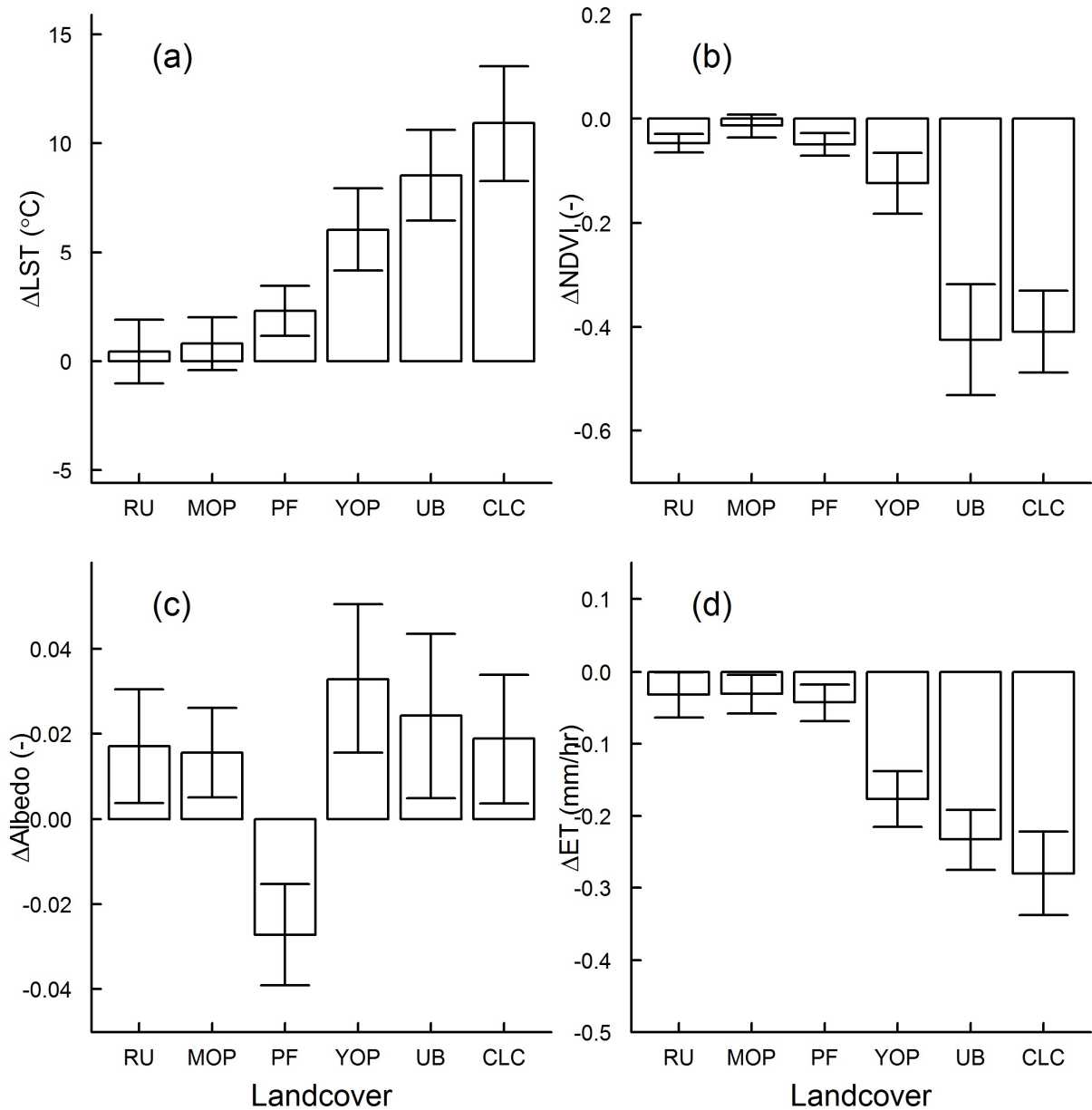
481 0.04 mm/hr, $\Delta ET_{UB-FO} = -0.23 \pm 0.04$ mm/hr, $\Delta ET_{CLC-FO} = -0.26 \pm 0.06$ mm/hr). The ΔET s

482 were significant ($p < 0.05$, post-hoc Tukey's HSD test). The SEBAL based LE estimates were

483 within the variability range of LE measurements from eddy covariance measurements under

484 similar meteorological conditions (see SI 3).

485



486
 487 **Fig. 4** Differences (mean \pm SD) in surface temperature (ΔLST), normalized difference
 488 vegetation index ($\Delta NDVI$), Albedo ($\Delta Albedo$) and Evapotranspiration (ΔET) between other
 489 land covers (RU, MOP, PF, YOP, UB and CLC) and forest (FO) in the Jambi province, derived
 490 from the Landsat LST image acquired on 19 June 2013 at 10:13 am local time.

491
 492 Albedo had a weaker influence on the LST ($\rho = 0.25$, $p < 0.05$) (Table 2) than NDVI and ET.
 493 As the thermal radiance band (L6) and the atmospherically corrected thermal band (Rc) were
 494 the basis for the LST calculation, the high correlation between L6 and NDVI ($\rho = -0.87$, $p <$

495 0.05) and between L6 and ET ($\rho = -0.98$, $p < 0.05$) resulted in a high correlation between LST
 496 and NDVI ($\rho = -0.88$) and between LST and ET ($\rho = -0.98$). The analysis showed that albedo,
 497 NDVI and ET were all significant predictors of LST ($F_{(3, 41586)} = 1 \times 10^6$, $p < 0.05$). ET was the
 498 strongest predictor of LST (stand. $\beta = -1.11$, $p < 0.05$). Albedo (stand. $\beta = -0.19$, $p < 0.05$,
 499 resp.) and NDVI (stand. $\beta = -0.19$, $p < 0.05$) were weaker predictors of LST.

500

501 **Table 2** Statistical analysis between biophysical variables (albedo (α), NDVI and ET) and
 502 Spectral Radiance band (L6), corrected thermal band (Rc) and Landsat surface temperature
 503 (LST).

Model		ρ	R^2	β	Stand. β	Model fit (R^2)	F-statistics
L6 ~ α + NDVI + ET	α	0.26	0.05	-2.94	-0.19	0.99	F (3, 41586) = 1.10×106, ***
	NDVI	-0.87	0.10	0.23	0.11		
	ET	-0.98	1.13	-4.00	-1.16		
Rc ~ α + NDVI + ET	α	0.25	0.05	-4.88	-0.20	0.99	F (3, 41586) = 1.79×106, ***
	NDVI	-0.88	0.04	0.16	0.05		
	ET	-0.98	1.00	-6.21	-1.10		
LST ~ α + NDVI + ET	α	0.25	0.05	-34.01	-0.19	0.99	F(3, 41586) = 2.3×106, ***
	NDVI	-0.88	0.05	1.30	0.05		
	ET	-0.98	1.00	-43.53	-1.11		

504 ***: $p = 2 \times 10^{-16}$

505 LM: Multiple linear regression analysis between LST (or L6 or Rc) and 3 biophysical variables:
 506 Albedo (α), NDVI and ET. ρ = correlation coefficient; R^2 : R-squared of the components; β =
 507 regression coefficient of the component; stand. β = standardized β ; Model fit (R^2): overall model
 508 fit of the multiple linear regression. The values in brackets are for the analysis between the
 509 biophysical variables and the corrected thermal band (Rc).

510

511 A separate analysis (Table S6.3, Supporting information S6) showed that ET was a strong
 512 predictor of LST for each land cover type in this study and that NDVI and albedo were minor
 513 predictors of LST.

514

515 3.3 Effects of land-use change on the provincial surface temperature in the past decades

516

517 The average annual LST of the province was characterized by a fluctuating but increasing trend
518 during daytimes (Fig. 5a and 5b) between 2000 and 2015. The average morning LST (10:30
519 am) increased by 0.07 °C per year ($R^2 = 0.59$; $p < 0.001$), the midday afternoon LST (13:30
520 local time) increased by 0.13 °C per year ($R^2 = 0.35$; $p = 0.02$) between 2003 and 2015. While
521 the daytime LST showed a clear increase, the night and evening LST (10:30 pm and 1:30 am,
522 Fig. 5c and 5d) trends were small showing a decrease of -0.02 °C ($R^2 = 0.29$; $p = 0.02$) and $-$
523 0.01 °C ($R^2 = 0.05$; $p = 0.51$) per year, respectively. The observed LST trends resulted in a total
524 LST increase of 1.05 °C and 1.56 °C in the morning (10:30 am) and afternoon (1:30 pm)
525 respectively and a total decrease of the province LST of 0.3 °C (10:30 pm) and 0.12 °C (1:30
526 am) at night over the period from 2000 to 2015.

527

528 In order to separate the effect of land use change from global climate warming, we used a site
529 constantly covered by forest over that period (from the forest sites we used in this study) as a
530 reference not directly affected by land cover changes. That site showed less changes in LST
531 than the entire province: only the mean morning LST (10:30 am) had a significant but small
532 trend with an increase by 0.03 °C per year ($R^2 = 0.21$, $p < 0.05$) resulting in a total LST increase
533 of the province of 0.45 °C between 2000 and 2015 (Fig. 5a). This LST warming is much smaller
534 than the overall warming at provincial level of 1.05 °C. The LST time series at other times
535 showed no significant trends: the mean afternoon LST (1:30 pm) with -0.05 °C per year ($R^2 =$
536 0.01 , $p = 0.31$) (Fig. 5b), the night and evening LST with 0.01 °C per year (Fig. 5c and 5d, $p =$
537 0.19 and $p = 0.65$, respectively).

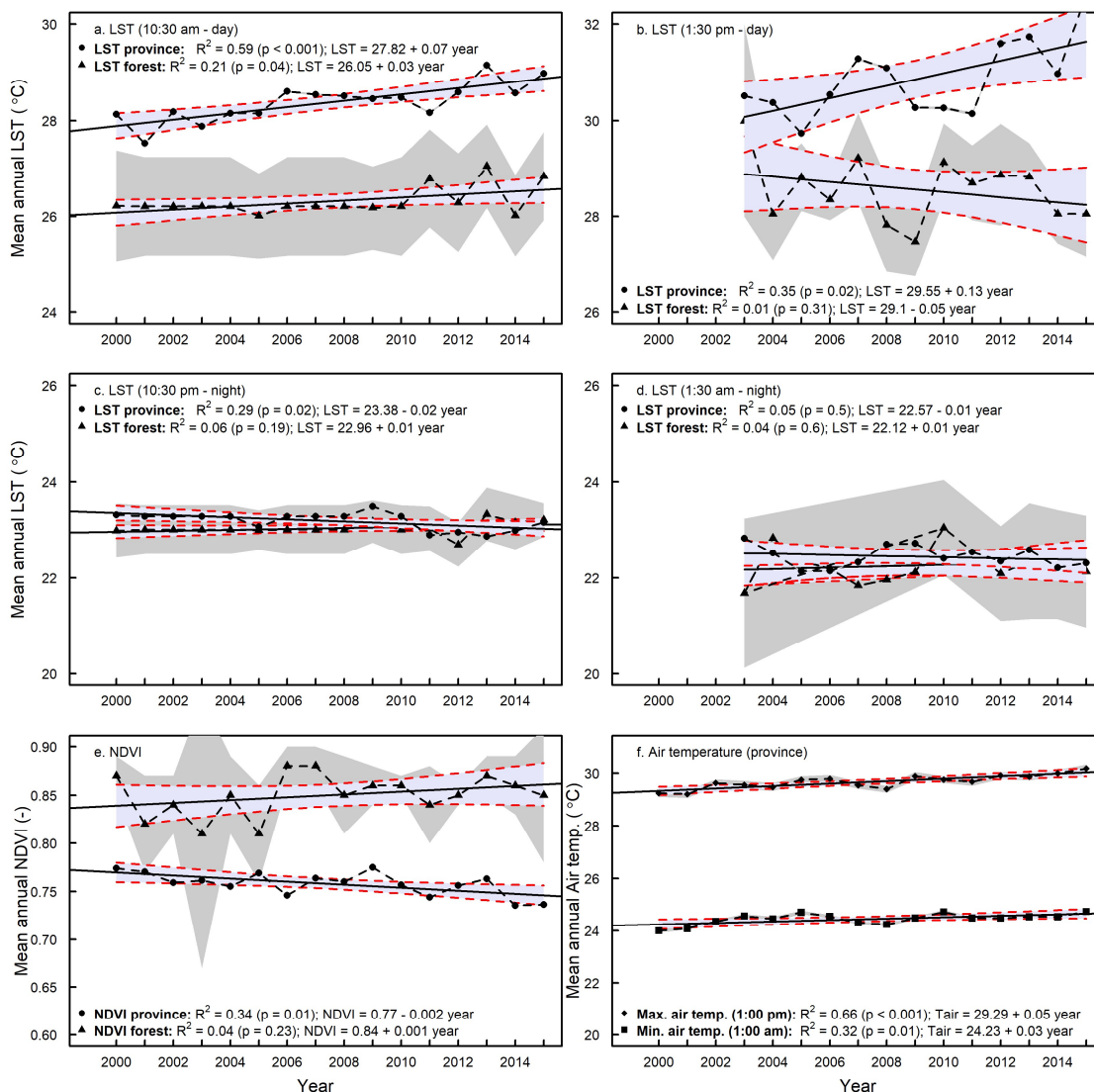
538

539 The mean annual NDVI of the province decreased by 0.002 per year, which resulted in a total
540 NDVI decrease of 0.03 ($R^2 = 0.34$; $p = 0.01$; Fig. 5e). The NDVI of the forest showed a small

541 but not significant increase of 0.001 per year ($R^2 = 0.04$, $p = 0.23$) (Fig. 5e) fluctuating around
 542 an NDVI of 0.84.

543

544 The mean annual midday air temperature (at 1:00 pm, local time, Fig. 5f) and the mean annual
 545 night air temperature (at 1:00 am, local time) increased every year by 0.05 °C and 0.03 °C,
 546 respectively resulting in a total air temperature increase of 0.75 °C ($R^2 = 0.66$, $p < 0.001$) and
 547 0.45 °C ($R^2 = 0.32$, $p = 0.014$) between 2000 and 2015 (Fig. 5f).



548

549 **Fig 5.** Mean annual LST (a – d), mean annual NDVI (e) and mean annual air temperature trends

550 (f) in the Jambi province between 2000 and 2015 derived from MODIS LST (5a. 10:30 am, 5b.

551 1:30 pm, 5c. 10:30 pm and 5d. 1:30 am, local time), MODIS NDVI and ERA Interim Daily air

552 temperature (1:00 am and 1:00 pm, local time) data sets respectively. Grey-shaded areas are the
553 confidence intervals of the means, blue-shaded areas are the confidence intervals of the
554 regression lines. MODIS LST time series for 1:30 pm and 1:30 am were available from the mid
555 of 2002; for this reason we used the complete years from 2003 till 2015.

556

557 **4 Discussion**

558

559 **4.1 Landsat LST compared to MODIS LST**

560

561 In our study we retrieved the surface temperature from a Landsat image and compared this with
562 MODIS LST. Our results showed a good agreement between both LSTs (Fig. 3), which is
563 comparable to other studies and thus gives confidence in our analysis. Bindhu et al. (2013)
564 found also a close relationship between MODIS LST and Landsat LST using the same
565 aggregation resampling technique as our method and found a R^2 of 0.90, a slope of 0.90, and
566 an intercept of 25.8 °C for LST, compared to our R^2 of 0.8, slope of 1.35 and intercept of –
567 11.58 °C (Fig. 3). Zhang and He (2013) validated Landsat LST with MODIS LST and also
568 found good agreements (RMSE 0.71 – 1.87 °C) between the two sensors, where we found a
569 RMSE of 1.71 °C. Nevertheless, there still are differences and slope versatility between the two
570 satellite sources. These differences are typically caused by differences between MODIS and
571 Landsat sensors in terms of (a) different sensor properties e.g. spatial and radiometric resolution
572 and sensor calibration; (b) geo-referencing and differences in atmospheric corrections (Li et al.,
573 2004); and (c) emissivity corrections i.e. the use of approximate equations to derive the
574 emissivity from the NDVI from Landsat's Red and NIR bands. Li et al. (2004) and Vlassova et
575 al. (2014) identified these same factors in their comparison of ASTER LST with MODIS LST
576 and Landsat LST with MODIS LST, respectively. Vlassova et al. (2014) found good
577 agreements between MODIS and Landsat LST, obtaining higher LST with MODIS than with

578 Landsat, which they attributed to the delay of 15 minutes in acquisition time between MODIS
579 and Landsat. MODIS LST is measured 15 minutes later and our results showed that MODIS
580 LSTs were indeed higher than Landsat LST. A comparison of MODIS LST with locally
581 measured canopy surface temperatures during the overpass time of MODIS also showed
582 agreement (Supporting information S7, Figure S7.1). The slope was possibly due to differences
583 in instrumentation and emissivity corrections and to scale issues, still this comparison could
584 corroborate the quality check of MODIS LST.

585 As the MODIS LST product is proven to be accurate within 1 °C (Silvério et al., 2015; Wan et
586 al., 2004) and has been intensively validated, the use of MODIS LST was a proper way to assess
587 the quality of our Landsat LST.

588

589 The errors from the different sources (such as atmospheric correction, emissivity correction,
590 resampling Landsat to MODIS resolution) are difficult to quantify. When we tested the impact
591 of atmospheric correction and emissivity errors on the LST from Landsat retrieval we found
592 that: (a) the overall patterns across different land use types did not change, (b) emissivity was
593 the most important factor, but the effects on LST retrieval were small and (c) errors due to
594 atmospheric correction parameters were small because there were minor differences between
595 default Atmospheric correction (ATCOR) parameters and ATCOR parameters derived with
596 actual local conditions (relative humidity (RH), air pressure and air temperature). Following
597 the method of Coll et al. (2009) and Jiang et al. (2015) we show that the use of the online
598 atmospheric correction parameter calculator is a good option provided that RH, air temperature
599 and air pressure measurements are available. We additionally compared locally measured air
600 temperatures with MODIS air temperature and found a good agreement (Supporting
601 information S8, Figure S8.1), which served as a verification that we used a correct air
602 temperature for the atmospheric correction parameter calculator.

603 Overall, our comparison of LST from Landsat against LST from MODIS and against ground
604 observations suggests that we are able to retrieve meaningful spatial and temporal patterns of
605 LST in the Jambi province.

606

607 **4.2 LST patterns across different land use and land cover (LULC) types**

608

609 The land cover types in our study covered a range of land surface types that develop after forest
610 conversion. This is the first study in this region that includes oil palm and rubber as land use
611 types that develop after forest conversion. The coolest temperatures were at the vegetated land
612 cover types while the warmest surface temperatures were on the non-vegetated surface types
613 like urban areas and bare land. Interestingly, the oil palm and rubber plantations were only
614 slightly warmer than the forests whereas the young oil palm plantations had clearly higher LST
615 than the other vegetated surfaces. For other parts of the world, Lim et al. (2005, 2008), Fall et
616 al. (2010) and Weng et al. (2004) also observed cooler temperatures for forests and the highest
617 surface temperatures for barren and urban areas.

618 In Indonesia, land transformation is often not instantaneous from forest to oil palm or rubber
619 plantation, but can be associated with several years of bare or abandoned land in-between (Sheil
620 et al., 2009). Oil palm plantations typically have a rotation cycle of 25 years, resulting in
621 repeating patterns with young plantations (Dislich et al., 2016). Given the large differences in
622 LST between forests and bare soils or young oil palm plantations that we observed, a substantial
623 warming effect of land transformation at regional scale is expected.

624

625 **4.3 Drivers of local differences between different land cover types**

626

627 All land cover types (except Acacia Plantation Forests) had a higher albedo than forest,
628 indicating that these land cover types absorbed less incoming solar radiation than forests.

629 Nevertheless, these land cover types were warmer than forests, suggesting that the albedo was
630 not the dominant variable explaining LST. Indeed, the statistical analysis showed that $ET \sim$
631 LST had a higher correlation than $albedo \sim LST$. The ΔETs were significant, underlying that
632 despite their higher albedo, all land cover types had higher LSTs than forests due to lower ET
633 rates than forests. Vice versa, forests that absorb more solar radiation due to the lower albedo,
634 have lower LST due to the higher ET they exhibit, hereby identifying evaporative cooling as
635 the main determinant of regulating the surface temperature of all vegetation cover types (Li et
636 al., 2015).

637

638 Both observational and modeling studies carried out in other geographic regions and with other
639 trajectories support our observations. Observational studies in the Amazonia by Lawrence and
640 Vandecar (2015) on the conversion of natural vegetation to crop or pasture land showed a
641 surface warming effect. Salazar et al. (2015) provided additional evidence that conversion of
642 forest to other types of land use in the Amazonia caused significant reductions in precipitation
643 and increases in surface temperatures.

644 Alkama and Cescatti (2016) and earlier studies by Loarie et al. (2011a, 2011b) showed that
645 tropical deforestation may increase LST. Croplands in the Amazonian regions were also
646 warmer than forests through the reduction of ET (Ban-Weiss et al., 2011; Feddema et al., 2005)
647 and that the climatic response strongly depends on changes in energy fluxes rather than on
648 albedo changes (Loarie et al., 2011a, 2011b). A study by Silvério et al. (2015) indeed found
649 that tropical deforestation changes the surface energy balance and water cycle and that the
650 magnitude of the change strongly depends on the land uses that follow deforestation. They
651 found that the LST was 6.4 °C higher over croplands and 4.3 °C higher over pasture lands
652 compared to the forest they replaced, as a consequence of energy balance shifts. Ban-Weiss et
653 al. (2011) and Davin and de Noblet-Ducoudré (2010) added that in addition to the reduction of
654 ET, the reduction of surface roughness most likely enhanced the substantial local warming.

655

656 Also for non-Amazonian regions, the replacement of forests by crops caused changes
657 comparable with our observations. In temperate Argentina, Houspanossian et al. (2013) found
658 that the replacement of dry forests by crops resulted in an increase of albedo and still forests
659 exhibited cooler canopies than croplands. The cooler canopies were a result of a higher
660 aerodynamic conductance that enhanced the capacity of tree canopies to dissipate heat into the
661 atmosphere, and to both latent and sensible heat fluxes operating simultaneously to cool forest
662 canopies.

663

664 In a global analysis Li et al. (2015) showed that tropical forests generally have a low albedo,
665 but still the net energy gain caused by solar energy absorption is offset by a greater latent heat
666 loss via higher ET and that in the tropical forests the high ET cooling completely offsets the
667 albedo warming. For China, this cooling effect was also shown by Peng et al. (2014) who
668 compared LST, albedo and ET of plantation forests, grassland and cropland with forests.

669

670 For the USA, Weng et al. (2004) and for China, Yue et al. (2007), using NDVI as an indicator
671 of vegetation abundance, also found that areas with a high mean NDVI had a lower LST than
672 areas with a low mean NDVI, therefore suggesting that vegetation abundance is an important
673 factor in controlling the LST through higher ET rates. Our result support their assumptions by
674 showing the high correlation between NDVI – LST and ET – LST.

675

676 Our findings are also supported by modelling studies. Beltrán-Przekurat et al. (2012) found for
677 the Southern Amazon that conversion of wooded vegetation to soy bean plantations caused an
678 increase of the LST due to decreased latent heat and increased sensible heat fluxes. Climate
679 models also show the same warming trends and land surface modelling also projects an increase
680 in surface temperatures following deforestation in the Brazilian Cerrado (Beltrán-Przekurat et

681 al., 2012; Loarie et al., 2011b). In a global analysis, Pongratz et al. (2006) showed a LST
682 increase of forest to cropland or pasture transitions, which was driven by a reduced roughness
683 length and an increased aerodynamic resistance, and that the temperature response is intensified
684 in forest to clear/bare land transitions (1.2 – 1.7 °C increase). Similar to observational studies,
685 the modelling results of Bathiany et al. (2010) show that ET is the main driver of temperature
686 changes in tropical land areas.

687

688 In order to understand the effects of deforestation on biophysical variables in Indonesia, our
689 study identifies the following mechanisms: (a) reduction of ET decreases surface cooling, (b)
690 reduced surface roughness reduces air mixing in the surface layer and thus vertical heat fluxes,
691 (c) changes in albedo change the net radiation, (d) changes in energy partitioning in sensible
692 and latent heat and heat storage. The effect is an increase of the mean temperatures leading to
693 warming effects in all tropical climatic zones (Alkama and Cescatti, 2016). We point here that
694 our study (1) included a ground heat flux, but did not take into account the storage of heat in
695 the soil and the release of stored heat out of the soil during the daily cycle and (2) that the
696 Landsat satellite image was obtained under cloud free conditions with high shortwave radiation
697 input and low fraction of diffuse radiation. Therefore, the LST retrieved on cloud free days
698 might be overestimated compared to cloudy days, as the differences in LST between land uses
699 are supposed to be lower when diffuse radiation increases.

700

701 Our study is the first to include the oil palm and rubber expansion in Indonesia. In Indonesia,
702 smallholders take 40% of the land under oil palm cultivation for their account (Dislich et al.,
703 2016). Since the landscape in the Jambi province is characterized by small-scale smallholder-
704 dominated mosaic including rubber and oil palm monocultures (Clough et al., 2016), studies
705 using medium to coarse resolution data are not able to capture the small scale changes and
706 processes at the small-scale level. By using high resolution Landsat data we were able to also

707 include the effects of land use change on biophysical variables and the underlying processes of
708 the small scale holder agriculture.

709

710 **4.4 Effects of land use change on the provincial surface temperature in the past decades**

711

712 The increases in mean surface temperature of the Jambi province were stronger during the
713 morning (10:30 am) and afternoon (1:30 pm) than during the evening (10:30 pm) and night
714 (1:30 am). Given that our results show a decrease of the NDVI in the same period, this suggests
715 that the observed increased trend of the day time province LST can be attributed to the land
716 cover changes that occurred. Our assumption that the observed decreasing NDVI trend is caused
717 by land conversions is supported by two different studies which reported that in the Jambi
718 province, between 2000 and 2011 (Drescher et al., 2016) and between 2000 and 2013 (Clough
719 et al., 2016), the forest area decreased and that the largest increases were for rubber, oil palm,
720 and agricultural and tree crop areas. The class ‘other land use types’, which includes urban
721 areas, showed a minor increase (around 1%), suggesting that the decrease in NDVI was most
722 likely caused by forest cover loss and not by urban expansion (see Supporting information,
723 Table S9). The same observations on LULC change in Indonesia were also supported by Lee
724 et al. (2011), Margono et al. (2012, 2014) and (Luskin et al., 2014). Luskin et al. (2014) showed
725 that in the Jambi province, during the period 2000 – 2010, forests decreased by 17% while oil
726 palm and rubber area increased by 85% and 19%, respectively.

727

728 Given these trends in LULC changes, the observed LST trends were most likely caused by
729 gradual decrease of forest cover loss at the expense of agriculture and croplands. Our
730 assumptions are supported by findings of Silvério et al. (2015), Costa et al. (2007), Oliveira et
731 al. (2013), Spracklen et al. (2012) and Salazar et al. (2015) which indicate that land use
732 transitions in deforested areas likely have a strong influence on regional climate. Alkama and

733 Cescatti's (2016) analysis show that biophysical effects of changes in forest cover can
734 substantially affect the local climate by altering the average temperature, which is consistent
735 with our observations and can be related to the observed land use change in the Jambi province.
736 As Indonesia has undergone high rates of forest cover loss from 2000 to 2012 (Margono et al.,
737 2014), these findings support our assumptions that the observed LST increase in the Jambi
738 province was most likely caused by the observed land use changes.

739

740 To separate the effect of global warming from land-use change induced warming, we
741 considered areas with permanent and large enough forests as reference where changes are
742 mainly due to global warming. We find that LST of forests show either no significant trends (at
743 1:30 pm, 10:30 pm, 1:30 am) or just a clearly smaller increase of 0.03 °C per year at 10:30 am.
744 The difference between the LST trend of the province and of the forest at 10:30 am was 0.04
745 °C per year, resulting in a Δ LST of 0.6 °C between the province and forest in the period 2000
746 and 2015. We point out that our MODIS analysis has a larger proportion of data from the dry
747 season compared from the wet season, as there were more cloud free conditions during the dry
748 season. Thus, our reported warming effect reflects cloud free conditions. During cloudy
749 conditions, particularly in the wet season, the warming effect is expected to be lower. A
750 seasonality analysis showed that the relationships in the dry season are stronger than for the wet
751 season (see Supporting information S10, fig. S10.1) which suggests that the warming is more
752 pronounced during the dry season compared to the wet season, which is reasonable as we have
753 more incoming radiation during the dry season.

754

755 Using the warming effects we found between forest and other land cover types (Δ LST, Fig. 4a)
756 and the observed land cover changes by Clough et al. (2016) and Drescher et al. (2016)
757 (Supporting Information S9, table S9.1 and S9.2) we estimated the contribution of all land cover
758 types (except forest) to the Δ LST of the province between 2000 and 2015 to be 0.51°C out of

759 0.6°C observed above, which also supports our assumption that the increase of the province
760 LST was by 85% driven by land cover changes (see Supporting Information 9, Table S9.1 &
761 S9.2: Land use change analysis), with clear cut areas having a large contribution as they have
762 the largest warming effect.

763

764 The observed small, but significant increase in LST of forests of 0.03 °C per year at 10:30 am
765 reflects a LST change independent to land cover changes, as the forest remained unchanged
766 over that time period. A potential driver of that LST increase is the general global air
767 temperature trend due to changes in radiative forcing or border effects (advection from warmer
768 land uses), which is similar to the 1994 - 2014 time series analysis of Kayet et al. (2016), who
769 showed a LST increase for all land cover types ranging from wasted land, agriculture land,
770 open forest, dense forest, water bodies and built up areas.

771

772 The observed trends of province air temperature (Fig. 5f) were significant, suggesting that a
773 general warming due to global and regional effects contributes to the observed warming at
774 province level during day and night time, but that it is smaller than the land cover change
775 induced effects (Supporting Information S9, Table S9.1 & S9.2) at provincial level (Fig. 5a and
776 5b).

777

778 In our long-term analysis on the regional effects of land use change we observed an increase in
779 the mean LST and mean air temperature in the 2000 - 2015 period, concurrent with a decrease
780 of the NDVI. The warming observed from MODIS LST data and from the air temperature
781 obtained from the independent ERA Interim Reanalysis in the Jambi province are most likely
782 caused by the observed decrease of the forest area and an increase oil palm, rubber and other
783 cash crop areas in the same period, with other effects such as radiative forcing changes and
784 additional natural effects playing a smaller role. Given the plan of the Indonesian government

785 to substantially expand oil palm production with a projected additional demand of 1 to 28 Mha
786 in 2020 (Wicke et al., 2011), the strong warming effect we show for Jambi province may serve
787 as an indication of future changes in LST for other regions of Indonesia that will undergo land
788 transformations towards oil palm plantations.

789 A recent study by Tölle et al. (2017) showed that for Southeast Asia, land use change at large
790 scale may increase not only surface temperature but also impact other aspects of local and
791 regional weather and climate occurring also in regions remote from the original landscape
792 disturbance. Their results also indicate that land clearings can amplify the response to climatic
793 extreme events such as El Niño Southern Oscillation (ENSO). The observed effects of land use
794 change on the biophysical variables may have implications for ecosystem services in the Jambi
795 province beyond a pure warming effect. The high precipitation in this region in combination
796 with the reduced vegetation cover of bare land and young oil palm plantations impose risks of
797 soil erosion caused by surface run off. Less water infiltrates in the soil, thereby decreasing the
798 soil water storage that may lead to low water availability in the dry season (Dislich et al., 2016;
799 Merten et al., 2016). High surface temperatures in combination with low water availability may
800 make the vegetation and the surroundings more vulnerable to fires.

801

802 **5 Conclusion**

803

804 In summary, we showed the importance of forests in regulating the local and regional climate.

805 We derived biophysical variables from satellite data, analyzed the biophysical impacts of
806 deforestation and on a local scale we found a general warming effect after forests are
807 transformed to cash or tree croplands (oil palm, rubber, acacia) in the Jambi province of
808 Sumatra. The warming effect after forest conversion results from the reduced evaporative
809 cooling, which was identified as the main determinant of regulating the surface temperature.

810 On a regional scale, we saw that the effects of land cover changes are reflected back in changes

811 of the LST, NDVI and air temperature of the Jambi province. The warming effect induced by
812 land cover change clearly exceeded the global warming effect. Understanding the effects of
813 land cover change on the biophysical variables may support policies regarding conservation of
814 the existing forests, planning and expansion of the oil palm plantations and possible
815 afforestation measures.

816

817

818 **Supporting Information**

819

820 Supporting information to this article is arranged as follows:

821

822 **S1. Surface temperature retrieval from Landsat thermal images**

823 **Table S1.1.** Steps in the retrieval of the surface temperature from Landsat TIR band

824 **Table S1.2.** LMIN and LMAX values for Landsat 7 ETM+

825 **Table S1.3.** Mean solar exo-atmospheric irradiance ($ESUN_{\lambda}$) for Landsat 7 ETM+

826

827 **S2. Atmospheric correction of the thermal band**

828 **Table S2.1.** Input and output parameters for/from NASA's online atmospheric correction
829 parameter calculator

830

831 **S3. ET from satellite images with SEBAL**

832 **Fig. S3.1** Analysis of the steps involved in deriving the input for deriving ET from Landsat
833 images with SEBAL

834 **Fig. S3.2** Comparison of ET derived from upper anchor and lower anchor pixels.

835 **Table S3.1.** u^* , rah , LE and H measured at a young and mature oil palm plantation

836

837 **S4. Mean LST, NDVI, Albedo and NDVI extracted for 7 land cover types**

838 **Fig. S4.1** Mean LST, NDVI, Albedo and NDVI extracted from Landsat LST images for 7
839 land cover types

840

841 **S5. Difference in LST, NDVI, albedo and ET between Forest (FO) and 6 other land cover
842 types**

843 **Fig. S5.1** Differences in LST (ΔLST), NDVI ($\Delta NDVI$), Albedo ($\Delta Albedo$) and
844 Evapotranspiration (ΔET) between other land covers (RU, MOP, PF, YOP, UB and CLC) and
845 forest (FO) in the Jambi province

846

847 **S6. Statistical analysis**

848 **Table S6.1** ANOVA statistics

849 **Table S6.2** Post-hoc Tukey HSD test statistics

850 **Table S6.3** The relation LST-Albedo-NDVI-ET separated by land cover type

851

852 **S7. Comparison of MODIS LST to in situ measured canopy LST**

853 **Fig. S7.1** MODIS LST compared to in situ measured canopy surface temperature.

854

855 **S8. Comparison of MODIS Air temperature with locally measured air temperature**

856 **Fig. S8.1** MODIS Air temperature compared with in situ measured air temperatures

857

858 **S9. Land use change analysis for the Jambi province for 2000 – 2010**

859 **Table S9.1** Land use change (1990) – 2000 – 2010

860 **Table S9.2** Contribution of land cover change to total LST increase

861

862 **S10. Seasonality analysis**

863 **Fig S10.1** Mean annual LST in the Jambi province between 2000 and 2015 derived from
864 MODIS LST during the wet and dry season.

865

866 *Author contributions.* Clifton R. Sabajo conducted the research, fieldwork an analysis and
867 prepared the manuscript, which was reviewed by Guerric le Maire, Tania June, Ana Meijide,
868 Olivier Roupsard and Alexander Knohl. Ana Meijide and Alexander Knohl provided the
869 meteorological data.

Competing interests. The authors declare that they have no conflict of interest.

870 *Acknowledgements.* This research was funded by the Erasmus Mundus Joint Doctorate
871 Programme Forest and Nature for Society (EMJD FONASO) and the German Research
872 Foundation (DFG) through the CRC 990 “EForTS, Ecological and Socioeconomic Functions
873 of Tropical Lowland Rainforest Transformation Systems (Sumatra, Indonesia)” (subproject
874 A03). A special thanks to Huta Julu Bagus Putra, a.k.a. Monang, for his assistance and
875 translation during the field work in Indonesia. The authors state to have no conflict of interest.

876

877

878 **References**

879

880 Alkama, R. and Cescatti, A.: Biophysical climate impacts of recent changes in global forest
881 cover, *Science*, 351(6273), 600–604, doi:10.1126/science.aac8083, 2016.

882 Ban-Weiss, G. A., Bala, G., Cao, L., Pongratz, J. and Caldeira, K.: Climate forcing and response
883 to idealized changes in surface latent and sensible heat, *Environ. Res. Lett.*, 6(3), 34032, 2011.

884 Barsi, J. A., Barker, J. L. and Schott, J. R.: An Atmospheric Correction Parameter Calculator
885 for a Single Thermal Band Earth-Sensing Instrument, *Geosci. Remote Sens. Symp. 2003*
886 *IGARSS 03 Proc. 2003 IEEE Int.*, 5, 3014–3016 vol.5, doi:10.1109/IGARSS.2003.1294665,
887 2003.

888 Barsi, J. A., Schott, J. R., Palluconi, F. D. and Hook, S. J.: Validation of a web-based
889 atmospheric correction tool for single thermal band instruments, in *Proc. SPIE, Earth Observing*
890 *Systems X*, vol. 5882, San Diego, California, USA., 2005.

891 Bastiaanssen, W. G. .: SEBAL-based sensible and latent heat fluxes in the irrigated Gediz
892 Basin, Turkey, *J. Hydrol.*, 229(1–2), 87–100, doi:10.1016/S0022-1694(99)00202-4, 2000.

893 Bastiaanssen, W. G. M., Menenti, M., Feddes, R. A. and Holtslag, A. A. M.: A remote sensing
894 surface energy balance algorithm for land (SEBAL) - 1. Formulation, *J. Hydrol.*, 212(1–4),
895 198–212, doi:10.1016/s0022-1694(98)00253-4, 1998a.

896 Bastiaanssen, W. G. M., Pelgrum, H., Wang, J., Ma, Y., Moreno, J. F., Roerink, G. J. and van
897 der Wal, T.: A remote sensing surface energy balance algorithm for land (SEBAL): Part 2:
898 Validation, *J. Hydrol.*, 212–213, 213–229, doi:10.1016/S0022-1694(98)00254-6, 1998b.

899 Bathiany, S., Claussen, M., Brovkin, V., Raddatz, T. and Gayler, V.: Combined biogeophysical
900 and biogeochemical effects of large-scale forest cover changes in the MPI earth system model,
901 *Biogeosciences*, 7(5), 1383–1399, doi:10.5194/bg-7-1383-2010, 2010.

902 Beltrán-Przekurat, A., Pielke Sr, R. A., Eastman, J. L. and Coughenour, M. B.: Modelling the
903 effects of land-use/land-cover changes on the near-surface atmosphere in southern South
904 America, *Int. J. Climatol.*, 32(8), 1206–1225, doi:10.1002/joc.2346, 2012.

905 Bindhu, V. M., Narasimhan, B. and Sudheer, K. P.: Development and verification of a non-
906 linear disaggregation method (NL-DisTrad) to downscale MODIS land surface temperature to
907 the spatial scale of Landsat thermal data to estimate evapotranspiration, *Remote Sens. Environ.*,
908 135, 118–129, doi:10.1016/j.rse.2013.03.023, 2013.

909 Boisier, J. P., de Noblet-Ducoudré, N. and Ciais, P.: Historical land-use-induced
910 evapotranspiration changes estimated from present-day observations and reconstructed land-
911 cover maps, *Hydrol. Earth Syst. Sci.*, 18(9), 3571–3590, doi:10.5194/hess-18-3571-2014, 2014.

912 Bridhikitti, A. and Overcamp, T. J.: Estimation of Southeast Asian rice paddy areas with
913 different ecosystems from moderate-resolution satellite imagery, *Agric. Ecosyst. Environ.*,
914 146(1), 113–120, doi:10.1016/j.agee.2011.10.016, 2012.

915 Bright, R. M., Zhao, K., Jackson, R. B. and Cherubini, F.: Quantifying surface albedo and other
916 direct biogeophysical climate forcings of forestry activities, *Glob. Change Biol.*, 21(9), 3246–
917 3266, doi:10.1111/gcb.12951, 2015.

- 918 Clough, Y., Krishna, V. V., Corre, M. D., Darras, K., Denmead, L. H., Meijide, A., Moser, S.,
 919 Musshoff, O., Steinebach, S., Veldkamp, E., Allen, K., Barnes, A. D., Breidenbach, N., Brose,
 920 U., Buchori, D., Daniel, R., Finkeldey, R., Harahap, I., Hertel, D., Holtkamp, A. M., Hörandl,
 921 E., Irawan, B., Jaya, I. N. S., Jochum, M., Klarner, B., Knohl, A., Kotowska, M. M.,
 922 Krashevskaya, V., Kreft, H., Kurniawan, S., Leuschner, C., Maraun, M., Melati, D. N.,
 923 Opfermann, N., Pérez-Cruzado, C., Prabowo, W. E., Rembold, K., Rizali, A., Rubiana, R.,
 924 Schneider, D., Tjitrosoedirdjo, S. S., Tjoa, A., Tschardtke, T. and Scheu, S.: Land-use choices
 925 follow profitability at the expense of ecological functions in Indonesian smallholder landscapes,
 926 *Nat. Commun.*, 7, 13137, 2016.
- 927 Coll, C., Wan, Z. and Galve, J. M.: Temperature-based and radiance-based validations of the
 928 V5 MODIS land surface temperature product, *J. Geophys. Res.*, 114(D20), 2009.
- 929 Coll, C., Galve, J. M., Sanchez, J. M. and Caselles, V.: Validation of Landsat-7/ETM+ Thermal-
 930 Band Calibration and Atmospheric Correction With Ground-Based Measurements, *Geosci.*
 931 *Remote Sens. IEEE Trans. On*, 48(1), 547–555, doi:10.1109/TGRS.2009.2024934, 2010.
- 932 Costa, M. H., Yanagi, S. N. M., Souza, P. J. O. P., Ribeiro, A. and Rocha, E. J. P.: Climate
 933 change in Amazonia caused by soybean cropland expansion, as compared to caused by
 934 pastureland expansion, *Geophys. Res. Lett.*, 34(7), doi:10.1029/2007GL029271, 2007.
- 935 Davin, E. L. and de Noblet-Ducoudré, N.: Climatic Impact of Global-Scale Deforestation:
 936 Radiative versus Nonradiative Processes, *J. Clim.*, 23(1), 97–112,
 937 doi:10.1175/2009JCLI3102.1, 2010.
- 938 Dee, D. P., Uppala, S. M., Simmons, A. J., Berrisford, P., Poli, P., Kobayashi, S., Andrae, U.,
 939 Balmaseda, M. A., Balsamo, G., Bauer, P., Bechtold, P., Beljaars, A. C. M., van de Berg, L.,
 940 Bidlot, J., Bormann, N., Delsol, C., Dragani, R., Fuentes, M., Geer, A. J., Haimberger, L.,
 941 Healy, S. B., Hersbach, H., Hólm, E. V., Isaksen, L., Kållberg, P., Köhler, M., Matricardi, M.,
 942 McNally, A. P., Monge-Sanz, B. M., Morcrette, J.-J., Park, B.-K., Peubey, C., de Rosnay, P.,
 943 Tavolato, C., Thépaut, J.-N. and Vitart, F.: The ERA-Interim reanalysis: configuration and
 944 performance of the data assimilation system, *Q. J. R. Meteorol. Soc.*, 137(656), 553–597,
 945 doi:10.1002/qj.828, 2011.
- 946 Dislich, C., Keyel, A. C., Salecker, J., Kisel, Y., Meyer, K. M., Auliya, M., Barnes, A. D.,
 947 Corre, M. D., Darras, K., Faust, H., Hess, B., Klasen, S., Knohl, A., Kreft, H., Meijide, A.,
 948 Nurdiansyah, F., Otten, F., Pe'er, G., Steinebach, S., Tarigan, S., Tölle, M. H., Tschardtke, T.
 949 and Wiegand, K.: A review of the ecosystem functions in oil palm plantations, using forests as
 950 a reference system, *Biol. Rev.*, doi:10.1111/brv.12295, 2016.
- 951 Drescher, J., Rembold, K., Allen, K., Beckschäfer, P., Buchori, D., Clough, Y., Faust, H., Fauzi,
 952 A. M., Gunawan, D., Hertel, D., Irawan, B., Jaya, I. N. S., Klarner, B., Kleinn, C., Knohl, A.,
 953 Kotowska, M. M., Krashevskaya, V., Krishna, V., Leuschner, C., Lorenz, W., Meijide, A., Melati,
 954 D., Nomura, M., Pérez-Cruzado, C., Qaim, M., Siregar, I. Z., Steinebach, S., Tjoa, A.,
 955 Tschardtke, T., Wick, B., Wiegand, K., Kreft, H. and Scheu, S.: Ecological and socio-economic
 956 functions across tropical land use systems after rainforest conversion, *Philos. Trans. R. Soc.*
 957 *Lond. B Biol. Sci.*, 371(1694), doi:10.1098/rstb.2015.0275, 2016.
- 958 Fall, S., Niyogi, D., Gluhovsky, A., Pielke, R. A., Kalnay, E. and Rochon, G.: Impacts of land
 959 use land cover on temperature trends over the continental United States: assessment using the
 960 North American Regional Reanalysis, *Int. J. Climatol.*, 30(13), 1980–1993,
 961 doi:10.1002/joc.1996, 2010.

- 962 Feddema, J. J., Oleson, K. W., Bonan, G. B., Mearns, L. O., Buja, L. E., Meehl, G. A. and
 963 Washington, W. M.: The Importance of Land-Cover Change in Simulating Future Climates,
 964 *Science*, 310(5754), 1674, doi:10.1126/science.1118160, 2005.
- 965 Hoffmann, W. A. and Jackson, R. B.: Vegetation–Climate Feedbacks in the Conversion of
 966 Tropical Savanna to Grassland, *J. Clim.*, 13(9), 1593–1602, doi:10.1175/1520-
 967 0442(2000)013<1593:VCFITC>2.0.CO;2, 2000.
- 968 Houspanossian, J., Nosoetto, M. and Jobbágy, E. G.: Radiation budget changes with dry forest
 969 clearing in temperate Argentina, *Glob. Change Biol.*, 19(4), 1211–1222,
 970 doi:10.1111/gcb.12121, 2013.
- 971 Idso, S. B. and Jackson, R. D.: Thermal radiation from the atmosphere, *J. Geophys. Res.*,
 972 74(23), 5397–5403, doi:10.1029/JC074i023p05397, 1969.
- 973 Jiang, Y., Fu, P. and Weng, Q.: Assessing the Impacts of Urbanization-Associated Land
 974 Use/Cover Change on Land Surface Temperature and Surface Moisture: A Case Study in the
 975 Midwestern United States, *Remote Sens.*, 7(4), doi:10.3390/rs70404880, 2015.
- 976 Kayet, N., Pathak, K., Chakrabarty, A. and Sahoo, S.: Spatial impact of land use/land cover
 977 change on surface temperature distribution in Saranda Forest, Jharkhand, *Model. Earth Syst.*
 978 *Environ.*, 2(3), 1–10, doi:10.1007/s40808-016-0159-x, 2016.
- 979 Lawrence, D. and Vandecar, K.: Effects of tropical deforestation on climate and agriculture,
 980 *Nat. Clim. Change*, 5(1), 27–36, 2015.
- 981 Lee, X., Goulden, M. L., Hollinger, D. Y., Barr, A., Black, T. A., Bohrer, G., Bracho, R., Drake,
 982 B., Goldstein, A., Gu, L., Katul, G., Kolb, T., Law, B. E., Margolis, H., Meyers, T., Monson,
 983 R., Munger, W., Oren, R., Paw U, K. T., Richardson, A. D., Schmid, H. P., Staebler, R., Wofsy,
 984 S. and Zhao, L.: Observed increase in local cooling effect of deforestation at higher latitudes,
 985 *Nature*, 479(7373), 384–387, doi:10.1038/nature10588, 2011.
- 986 van Leeuwen, T. T., Frank, A. J., Jin, Y., Smyth, P., Goulden, M. L., van der Werf, G. R. and
 987 Randerson, J. T.: Optimal use of land surface temperature data to detect changes in tropical
 988 forest cover, *J. Geophys. Res. Biogeosciences*, 116(G2), doi:10.1029/2010JG001488, 2011.
- 989 Li, F., Jackson, T. J., Kustas, W. P., Schmugge, T. J., French, A. N., Cosh, M. H. and Bindlish,
 990 R.: Deriving land surface temperature from Landsat 5 and 7 during SMEX02/SMACEX, 2002
 991 *Soil Moisture Exp. SMEX02*, 92(4), 521–534, doi:10.1016/j.rse.2004.02.018, 2004.
- 992 Li, Y., Zhao, M., Motesharrei, S., Mu, Q., Kalnay, E. and Li, S.: Local cooling and warming
 993 effects of forests based on satellite observations, *Nat. Commun.*, 6 [online] Available from:
 994 <http://dx.doi.org/10.1038/ncomms7603>, 2015.
- 995 Liang, S.: Narrowband to broadband conversions of land surface albedo I: Algorithms, *Remote*
 996 *Sens. Environ.*, 76(2), 213–238, doi:10.1016/S0034-4257(00)00205-4, 2000.
- 997 Lim, Y.-K., Cai, M., Kalnay, E. and Zhou, L.: Observational evidence of sensitivity of surface
 998 climate changes to land types and urbanization, *Geophys. Res. Lett.*, 32(22),
 999 doi:10.1029/2005GL024267, 2005.
- 1000 Lim, Y.-K., Cai, M., Kalnay, E. and Zhou, L.: Impact of Vegetation Types on Surface
 1001 Temperature Change, *J. Appl. Meteorol. Climatol.*, 47(2), 411–424, 2008.

- 1002 Loarie, S. R., Lobell, D. B., Asner, G. P., Mu, Q. and Field, C. B.: Direct impacts on local
1003 climate of sugar-cane expansion in Brazil, *Nat. Clim. Change*, 1(2), 105–109,
1004 doi:10.1038/nclimate1067, 2011a.
- 1005 Loarie, S. R., Lobell, D. B., Asner, G. P. and Field, C. B.: Land-Cover and Surface Water
1006 Change Drive Large Albedo Increases in South America, *Earth Interact.*, 15(7), 1–16, 2011b.
- 1007 Longobardi, P., Montenegro, A., Beltrami, H. and Eby, M.: Deforestation Induced Climate
1008 Change: Effects of Spatial Scale, *PLoS ONE*, 11(4), e0153357,
1009 doi:10.1371/journal.pone.0153357, 2016.
- 1010 Luskin, M. S., Christina, E. D., Kelley, L. C. and Potts, M. D.: Modern Hunting Practices and
1011 Wild Meat Trade in the Oil Palm Plantation-Dominated Landscapes of Sumatra, Indonesia,
1012 *Hum. Ecol.*, 42(1), 35–45, doi:10.1007/s10745-013-9606-8, 2014.
- 1013 Mahmood, R., Pielke, R. A., Hubbard, K. G., Niyogi, D., Dirmeyer, P. A., McAlpine, C.,
1014 Carleton, A. M., Hale, R., Gameda, S., Beltrán-Przekurat, A., Baker, B., McNider, R., Legates,
1015 D. R., Shepherd, M., Du, J., Blanken, P. D., Frauenfeld, O. W., Nair, U. S. and Fall, S.: Land
1016 cover changes and their biogeophysical effects on climate, *Int. J. Climatol.*, 34(4), 929–953,
1017 doi:10.1002/joc.3736, 2014.
- 1018 Margono, B. A., Turubanova, S., Zhuravleva, I., Potapov, P., Tyukavina, A., Baccini, A., Goetz,
1019 S. and Hansen, M. C.: Mapping and monitoring deforestation and forest degradation in Sumatra
1020 (Indonesia) using Landsat time series data sets from 1990 to 2010, *Environ. Res. Lett.*, 7(3),
1021 34010, doi:10.1088/1748-9326/7/3/034010, 2012.
- 1022 Margono, B. A., Potapov, P. V., Turubanova, S., Stolle, F. and Hansen, M. C.: Primary forest
1023 cover loss in Indonesia over 2000-2012, *Nat. Clim Change*, 4(8), 730–735, 2014.
- 1024 Marlier, M. E., DeFries, R., Pennington, D., Nelson, E., Ordway, E. M., Lewis, J., Koplitz, S.
1025 N. and Mickley, L. J.: Future fire emissions associated with projected land use change in
1026 Sumatra, *Glob. Change Biol.*, 21(1), 345–362, doi:10.1111/gcb.12691, 2015.
- 1027 Meijide, A., Röhl, A., Fan, Y., Herbst, M., Niu, F., Tiedemann, F., June, T., Rauf, A., Hölscher,
1028 D. and Knohl, A.: Controls of water and energy fluxes in oil palm plantations: Environmental
1029 variables and oil palm age, *Agric. For. Meteorol.*, 239, 71–85,
1030 doi:10.1016/j.agrformet.2017.02.034, 2017.
- 1031 Merten, J., Röhl, A., Guillaume, T., Meijide, A., Tarigan, S., Agusta, H., Dislich, C., Dittrich,
1032 C., Faust, H., Gunawan, D., Hein, J., Hendrayanto, Knohl, A., Kuzyakov, Y., Wiegand, K. and
1033 Hölscher, D.: Water scarcity and oil palm expansion: social views and environmental processes,
1034 *Ecol. Soc.*, 21(2), doi:10.5751/ES-08214-210205, 2016.
- 1035 Miettinen, J., Shi, C. and Liew, S. C.: Deforestation rates in insular Southeast Asia between
1036 2000 and 2010, *Glob. Change Biol.*, 17(7), 2261–2270, 2011.
- 1037 Miettinen, J., Hooijer, A., Wang, J., Shi, C. and Liew, S. C.: Peatland degradation and
1038 conversion sequences and interrelations in Sumatra, *Reg. Environ. Change*, 12(4), 729–737,
1039 doi:10.1007/s10113-012-0290-9, 2012.

- 1040 Mildrexler, D. J., Zhao, M. and Running, S. W.: A global comparison between station air
1041 temperatures and MODIS land surface temperatures reveals the cooling role of forests, *J.*
1042 *Geophys. Res. Biogeosciences*, 116(G3), doi:10.1029/2010JG001486, 2011.
- 1043 Noretto, M. D., Jobbágy, E. G. and Paruelo, J. M.: Land-use change and water losses: the case
1044 of grassland afforestation across a soil textural gradient in central Argentina, *Glob. Change*
1045 *Biol.*, 11(7), 1101–1117, doi:10.1111/j.1365-2486.2005.00975.x, 2005.
- 1046 Oliveira, L. J. C., Costa, M. H., Soares-Filho, B. S. and Coe, M. T.: Large-scale expansion of
1047 agriculture in Amazonia may be a no-win scenario, *Environ. Res. Lett.*, 8(2), 24021, 2013.
- 1048 Peng, S.-S., Piao, S., Zeng, Z., Ciais, P., Zhou, L., Li, L. Z. X., Myneni, R. B., Yin, Y. and
1049 Zeng, H.: Afforestation in China cools local land surface temperature, *Proc. Natl. Acad. Sci.*,
1050 111(8), 2915–2919, 2014.
- 1051 Pongratz, J., Bounoua, L., DeFries, R. S., Morton, D. C., Anderson, L. O., Mauser, W. and
1052 Klink, C. A.: The Impact of Land Cover Change on Surface Energy and Water Balance in Mato
1053 Grosso, Brazil, *Earth Interact.*, 10(19), 1–17, 2006.
- 1054 Salazar, A., Baldi, G., Hirota, M., Syktus, J. and McAlpine, C.: Land use and land cover change
1055 impacts on the regional climate of non-Amazonian South America: A review, *Glob. Planet.*
1056 *Change*, 128, 103–119, doi:10.1016/j.gloplacha.2015.02.009, 2015.
- 1057 Salazar, A., Katzfey, J., Thatcher, M., Syktus, J., Wong, K. and McAlpine, C.: Deforestation
1058 changes land–atmosphere interactions across South American biomes, *Glob. Planet. Change*,
1059 139, 97–108, doi:10.1016/j.gloplacha.2016.01.004, 2016.
- 1060 Sheil, D., Casson, A., Meijaard, E., Van Noordwijk, M., Gaskell, J., Sunderland-Groves, J.,
1061 Wertz, K. and Kanninen, M.: The impacts and opportunities of oil palm in Southeast Asia: What
1062 do we know and what do we need to know?, Center for International Forestry Research
1063 (CIFOR), Bogor, Indonesia., 2009.
- 1064 Silvério, D. V., Brando, P. M., Macedo, M. N., Beck, P. S. A., Bustamante, M. and Coe, M. T.:
1065 Agricultural expansion dominates climate changes in southeastern Amazonia: the overlooked
1066 non-GHG forcing, *Environ. Res. Lett.*, 10(10), 104015, 2015.
- 1067 Snyder, W. C., Wan, Z., Zhang, Y. and Feng, Y.-Z.: Classification-based emissivity for land
1068 surface temperature measurement from space, *Int. J. Remote Sens.*, 19(14), 2753–2774,
1069 doi:10.1080/014311698214497, 1998.
- 1070 Sobrino, J. A., Jiménez-Muñoz, J. C. and Paolini, L.: Land surface temperature retrieval from
1071 LANDSAT TM 5, *Remote Sens. Environ.*, 90(4), 434–440, doi:10.1016/j.rse.2004.02.003,
1072 2004.
- 1073 Sobrino, J. A., Jiménez-Muñoz, J. C., Zarco-Tejada, P. J., Sepulcre-Cantó, G. and de Miguel,
1074 E.: Land surface temperature derived from airborne hyperspectral scanner thermal infrared data,
1075 *Remote Sens. Environ.*, 102(1–2), 99–115, doi:10.1016/j.rse.2006.02.001, 2006.
- 1076 Sobrino, J. A., Jimenez-Muoz, J. C., Soria, G., Romaguera, M., Guanter, L., Moreno, J., Plaza,
1077 A. and Martinez, P.: Land Surface Emissivity Retrieval From Different VNIR and TIR Sensors,
1078 *Geosci. Remote Sens. IEEE Trans. On*, 46(2), 316–327, doi:10.1109/TGRS.2007.904834,
1079 2008.

- 1080 Spracklen, D. V., Arnold, S. R. and Taylor, C. M.: Observations of increased tropical rainfall
1081 preceded by air passage over forests, *Nature*, 489(7415), 282–285, doi:10.1038/nature11390,
1082 2012.
- 1083 Tölle, M. H., Engler, S. and Panitz, H.-J.: Impact of Abrupt Land Cover Changes by Tropical
1084 Deforestation on Southeast Asian Climate and Agriculture, *J. Clim.*, 30(7), 2587–2600,
1085 doi:10.1175/JCLI-D-16-0131.1, 2017.
- 1086 Verstraeten, W. W., Veroustraete, F. and Feyen, J.: Estimating evapotranspiration of European
1087 forests from NOAA-imagery at satellite overpass time: Towards an operational processing
1088 chain for integrated optical and thermal sensor data products, *Remote Sens. Environ.*, 96(2),
1089 256–276, doi:10.1016/j.rse.2005.03.004, 2005.
- 1090 Vlassova, L., Perez-Cabello, F., Nieto, H., Martín, P., Riaño, D. and de la Riva, J.: Assessment
1091 of Methods for Land Surface Temperature Retrieval from Landsat-5 TM Images Applicable to
1092 Multiscale Tree-Grass Ecosystem Modeling, *Remote Sens.*, 6(5), doi:10.3390/rs6054345,
1093 2014.
- 1094 Voogt, J. A. and Oke, T. R.: Effects of urban surface geometry on remotely-sensed surface
1095 temperature, *Int. J. Remote Sens.*, 19(5), 895–920, doi:10.1080/014311698215784, 1998.
- 1096 Wan, Z., Zhang, Y., Zhang, Q. and Li, Z.-L.: Quality assessment and validation of the MODIS
1097 global land surface temperature, *Int. J. Remote Sens.*, 25(1), 261–274,
1098 doi:10.1080/0143116031000116417, 2004.
- 1099 Weng, Q.: Thermal infrared remote sensing for urban climate and environmental studies:
1100 Methods, applications, and trends, *ISPRS J. Photogramm. Remote Sens.*, 64(4), 335–344,
1101 doi:10.1016/j.isprsjprs.2009.03.007, 2009.
- 1102 Weng, Q., Lu, D. and Schubring, J.: Estimation of land surface temperature–vegetation
1103 abundance relationship for urban heat island studies, *Remote Sens. Environ.*, 89(4), 467–483,
1104 doi:10.1016/j.rse.2003.11.005, 2004.
- 1105 Wicke, B., Sikkema, R., Dornburg, V. and Faaij, A.: Exploring land use changes and the role
1106 of palm oil production in Indonesia and Malaysia, *Land Use Policy*, 28(1), 193–206, 2011.
- 1107 Wukelic, G. E., Gibbons, D. E., Martucci, L. M. and Foote, H. P.: Radiometric calibration of
1108 Landsat Thematic Mapper thermal band, *Remote Sens. Environ.*, 28(0), 339–347,
1109 doi:10.1016/0034-4257(89)90125-9, 1989.
- 1110 Yue, W., Xu, J., Tan, W. and Xu, L.: The relationship between land surface temperature and
1111 NDVI with remote sensing: application to Shanghai Landsat 7 ETM+ data, *Int. J. Remote Sens.*,
1112 28(15), 3205–3226, doi:10.1080/01431160500306906, 2007.
- 1113 Zhang, Z. and He, G.: Generation of Landsat surface temperature product for China, 2000–
1114 2010, *Int. J. Remote Sens.*, 34(20), 7369–7375, doi:10.1080/01431161.2013.820368, 2013.
- 1115 Zhou, X. and Wang, Y.-C.: Dynamics of Land Surface Temperature in Response to Land-
1116 Use/Cover Change, *Geogr. Res.*, 49(1), 23–36, doi:10.1111/j.1745-5871.2010.00686.x, 2011.
- 1117
- 1118

